Provided for non-commercial research and education use.
Not for reproduction, distribution or commercial use.

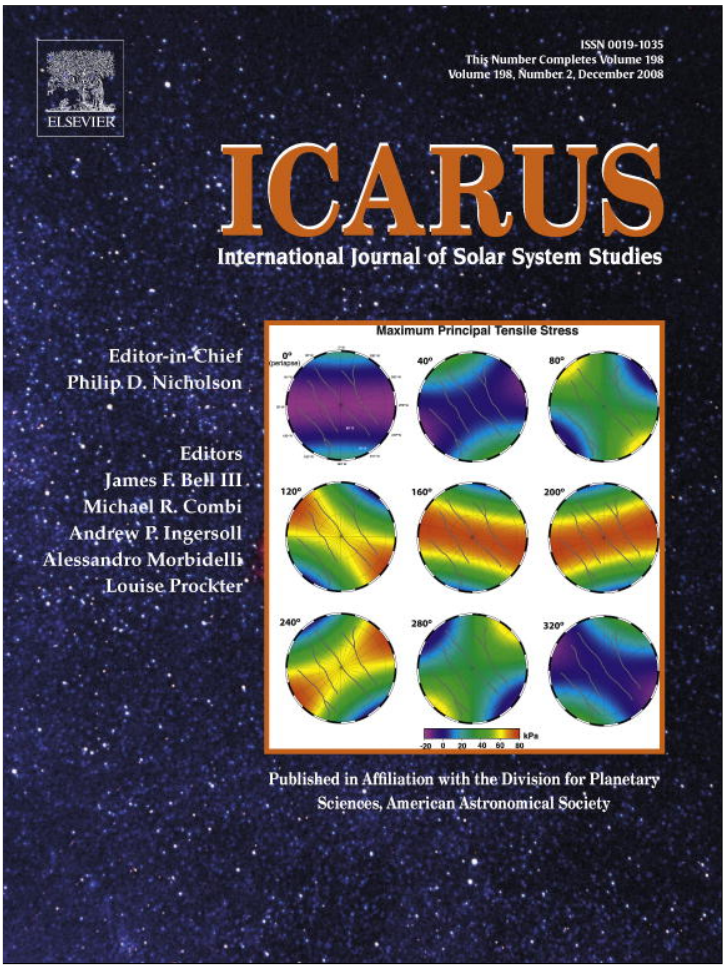

This article appeared in a journal published by Elsevier. The attached copy is furnished to the author for internal non-commercial research and education use, including for instruction at the authors institution and sharing with colleagues.

Other uses, including reproduction and distribution, or selling or licensing copies, or posting to personal, institutional or third party websites are prohibited.

In most cases authors are permitted to post their version of the article (e.g. in Word or Tex form) to their personal website or institutional repository. Authors requiring further information regarding Elsevier's archiving and manuscript policies are encouraged to visit:

http://www.elsevier.com/copyright

Author's personal copy

Icarus 198 (2008) 384–399

Contents lists available at ScienceDirect

Icarus

www.elsevier.com/locate/icarus

The production of Ganymede's magnetic field

Michael T. Bland [a,*], Adam P. Showman [a], Gabriel Tobie [b,c]

[a] Department of Planetary Sciences, Lunar and Planetary Laboratory, University of Arizona, Tucson, AZ 85721, USA
[b] Université Nantes Atlantique, Laboratoire de Planétologie et Géodynamique de Nantes, 2, rue de la Houssiniére, 44322 Nantes cedex 03, France
[c] CNRS, UMR-6112, 2, rue de la Houssiniére, 44322 Nantes cedex 03, France

ARTICLE INFO

Article history:
Received 31 January 2008
Revised 11 June 2008
Available online 26 August 2008

Keywords:
Ganymede
Magnetic fields
Thermal histories
Resonances, orbital

ABSTRACT

One of the great discoveries of NASA's Galileo mission was the presence of an intrinsically produced magnetic field at Ganymede. Generation of the relatively strong (750 nT) field likely requires dynamo action in Ganymede's metallic core, but how such a dynamo has been maintained into the present epoch remains uncertain. Using a one-dimensional, three layer thermal model of Ganymede, we find that magnetic field generation can only occur if the sulfur mass fraction in Ganymede's core is very low ($\lesssim$3%) or very high ($\gtrsim$21%), and the silicate mantle can cool rapidly (i.e. it has a viscosity like wet olivine). However, these requirements are not necessarily compatible with cosmochemical and physical models of the satellite. We therefore investigate an alternative scenario for producing Ganymede's magnetic field in which passage through an eccentricity pumping Laplace-like resonance in Ganymede's past enables present day dynamo action in the metallic core. If sufficient tidal dissipation occurs in Ganymede's silicate mantle during resonance passage, silicate temperatures can undergo a runaway which prevents the core from cooling until the resonance passage ends. The rapid silicate and core cooling that follows resonance escape triggers dynamo action via thermal and/or compositional convection. To test the feasibility of this mechanism we couple our thermal model with an orbital evolution model to examine the effects of resonance passage on Ganymede's silicate mantle and metallic core. We find that, contrary to expectations, there are no physically plausible scenarios in which tidal heating in the silicates is sufficient to cause the thermal runaway necessary to prevent core cooling. These findings are robust to variations in the silicate rheology, tidal dissipation factor of Jupiter (Q_J), structure of the ice shell, and the inclusion of partial melting in the silicate mantle. Resonance passage therefore appears unlikely to explain Ganymede's magnetic field and we must appeal to the special conditions described above to explain the presence of the field.

© 2008 Elsevier Inc. All rights reserved.

1. Background

Ganymede is unique among the satellites of the Solar System in that it has an intrinsic magnetic field (Kivelson et al., 1996; Gurnett et al., 1996; Williams et al., 1997) while other large satellites do not. Analysis of magnetometer data taken during the Galileo spacecraft's four close Ganymede flybys suggest that the field consists of a Ganymede-centered dipole tilted 10° with respect to the rotation axis (Kivelson et al., 1996). With an equatorial surface-field strength of 750 nT, the field creates a mini-magnetosphere ~2 Ganymede radii in extent within Jupiter's larger magnetosphere (Kivelson et al., 1996, 1997, 1998).

The strength of the observed field and Ganymede's high degree of central condensation [$C/MR^2 = 0.3115$ where C is the axial moment of inertia, and M and R are the satellite mass and radius respectively (Anderson et al., 1996; Schubert et al., 2004)] suggest that dynamo action within a metallic core generates the magnetic field (Schubert et al., 1996; Sarson et al., 1997). Other field producing mechanisms are largely inconsistent with observations. The strength of the field, which is significantly greater than Jupiter's field at Ganymede's location, makes production by induction [the mechanism that produces the fields of Europa and Callisto (Khurana et al., 1998; Kivelson et al., 1999, 2000; Zimmer et al., 2000)] unlikely (Schubert et al., 1996). Ganymede's observed field may, in fact, include an induced field component generated in a conducting layer (likely an ocean) at ~150 km depth; however, modeling indicates that this component is small (Kivelson et al., 2002). Additionally, the unrealistically high fluid velocities (1 m s^{-1}) required to produce a dynamo in a thick, electrically conducting ocean make such a mechanism unfeasible (Schubert et al., 1996). Furthermore, producing the observed field via remnant magnetization of Ganymede's rocky mantle requires making rather favorable assumptions regarding the magnetic properties of the rocky materials and requires that a strong dynamo-generated field existed earlier in Ganymede's history (Crary and Bagenal, 1998).

* Corresponding author. Now at: Department of Earth and Planetary Science, Washington University, St. Louis, MO 63130, USA. Fax: +1 (314) 935 7361.
E-mail address: mbland@levee.wustl.arizona.edu (M.T. Bland).

0019-1035/$ – see front matter © 2008 Elsevier Inc. All rights reserved.
doi:10.1016/j.icarus.2008.07.011

Author's personal copy

While we cannot eliminate the mechanism entirely, it seems less plausible than a dynamo generated magnetic field (Schubert et al., 1996).

The dynamo mechanism for magnetic field production requires that fluid motions occur within an electrically conducting medium such as a fluid metallic core. In a planetary dynamo, buoyancy driven convection provides this motion [Malkus (1963) and Vanyo et al. (1995) have also suggested that precession can drive motion within a fluid core, however its relevance to dynamo generation is debatable (e.g. Rochester et al., 1975; Loper, 1975)]. In the absence of an inner solid core, thermal buoyancy alone must drive convection. The requirement for convection in this case is simply that the heat flux out of the core (F_{total}) is greater than the maximum heat flux that can be carried conductively ($F_{\text{cond,ad}}$) (i.e. the heat flux conducted along the core adiabat). Thus, for convection (Stevenson, 2003)

$$F_{\text{total}} > F_{\text{cond,ad}} \equiv k_c \frac{\alpha_c g_c T_{\text{cmb}}}{c_{p,c}}, \tag{1}$$

where k_c is the thermal conductivity, α_c is the thermal expansivity, $g_c \approx 1.3\ \text{m s}^{-2}$ is the local gravitational acceleration (cf. Sohl et al., 2002), T_{cmb} is the temperature at the core–mantle boundary, and $c_{p,c}$ is the specific heat at constant pressure. Equating the minimum required heat flux (Eq. (1)) to the cooling rate of the core yields a minimum cooling rate required to maintain thermal convection

$$\left(\frac{\text{d}T}{\text{d}t}\right)_{\text{min}} = \frac{3k_c\alpha_c g_c T_{\text{cmb}}}{R_c \rho_c c_{p,c}^2}, \tag{2}$$

where R_c and ρ_c are the radius and density of the core respectively. For parameters appropriate to Ganymede (Table 1) and $T_{\text{cmb}} = 2000$ K, the minimum required cooling rate is $\sim 250\ \text{K Ga}^{-1}$. If we assume secular cooling of Ganymede's core associated with the decline in radiogenic heating over the age of the Solar System, the present cooling rate falls well short of the minimum requirement (see Section 3) and a dynamo driven by present-day thermal convection appears unlikely.

To maintain a planetary dynamo, it is necessary but not sufficient that fluid motion occurs in a planetary core. In addition, a self-sustained planetary dynamo requires that convection can supply sufficient power to overcome losses due to ohmic dissipation of the field (e.g. Stevenson et al., 1983; Buffett, 2002). The ohmic dissipation Φ can be approximated by (Buffett, 2002)

$$\Phi = \left(\frac{\eta \bar{B}^2}{\mu_\circ L^2}\right)\frac{4}{3}\pi R_c^3, \tag{3}$$

where $\eta \sim 2\ \text{m}^2\,\text{s}^{-1}$ is the magnetic diffusivity, $\bar{B}$ is the average strength of the field at the core–mantle boundary, $\mu_\circ = 4\pi \times 10^{-7}\ \text{N A}^{-1}$ is the magnetic permeability, and L is the length scale for convection (a free parameter). Assuming a core radius of 700 km, and a convective length-scale equal to ~10% of the core radius we find $\Phi = 10^8$ W, consistent with the strength of Ganymede's magnetic field extrapolated to the core–mantle boundary. Because of the uncertainty in the radius of Ganymede's core and the length scale for convection, Φ may vary by an order of magnitude. Such variations do not affect our basic conclusions. The power requirement (W) for sustaining a dynamo is then (Stevenson et al., 1983)

$$P_B = 4\pi R_c^2 \frac{k_c\alpha_c g_c T_{\text{cmb}}}{c_{p,c}} + \frac{\Phi}{\epsilon} - \left(\frac{E_G}{\epsilon} + L_{Fe}\right)\frac{\text{d}m_{ic}}{\text{d}t}, \tag{4}$$

where ϵ is a Carnot-like efficiency factor (~0.05; Buffett et al., 1996), E_G is the gravitational energy per unit mass released by inner core formation, L_{Fe} is the latent heat of iron, and $\text{d}m_{ic}/\text{d}t$, is the rate at which the mass of the inner core increases. The first term on the right-hand side of Eq. (4) is simply the power lost from the core by conduction as given in Eq. (1); the second term is the additional power required to overcome ohmic dissipation; the third term is the power provided by compositional convection (see below) and is zero in the absence of an inner core.

Whether thermal convection can occur or not, cooling of the core can lead to the formation of a solid inner core. Inner core growth provides an additional source of energy and buoyancy in the core as heavy elements (e.g. Fe/Ni) freeze out, releasing latent heat, and light elements (e.g. sulfur) are expelled upward, releasing gravitational energy. Earth's magnetic dynamo appears to require such compositionally driven convection (e.g. Verhoogen, 1961; Braginsky, 1963; Gubbins, 1977; Loper, 1978a, 1978b; Lister and Buffett, 1995; Buffett et al., 1996; Gubbins et al., 2004), and it may play a similar role in driving Ganymede's core dynamo (Kuang and Stevenson, 1996; McKinnon, 1996; Hauck et al., 2006). Sulfur is a likely candidate for the light alloying material in Ganymede's core (e.g. McKinnon, 1996; Scott et al., 2002; Schubert et al., 2004). While elements such as oxygen are also plausible components (e.g. McKinnon and Desai, 2003), the inclusion of such a complex core chemistry is beyond the scope of the present work.

Equation (4) indicates that inner core formation relaxes the power requirements on the dynamo. However, whether compositional convection can account for Ganymede's dynamo remains unclear. In a detailed investigation of compositional convection's impact on the evolution of Ganymede's core, Hauck et al. (2006) used scaling arguments to calculate the magnetic Reynolds number ($Re_m = u\mathcal{L}/\eta$ where u is the flow velocity and $\mathcal{L}$ is the thickness of the convecting layer) associated with compositional convection. When one accounts for the fact that the inner core is ~50% of the total core radius after 4.6 Ga (see Hauck et al., 2006), then Re_m due to compositionally driven convection in Ganymede is ≈35. However, numerical investigations indicate that convectively-driven, self-sustained dynamos require a magnetic Reynolds number of 40 to 50 (Olson and Christensen, 2006; Christensen and Aubert, 2006). Compositional convection's ability to maintain Ganymede's dynamo over geologic time therefore appears marginal.

Furthermore, inner core formation on Ganymede may occur in a novel way relative to the Earth. In contrast to melting relations in the Fe–FeS system at high pressures (e.g. Boehler, 1996; Usselman, 1975), experimental work at low pressures (<14 GPa) indicate that, for sulfur concentrations greater than ~3%, the melting curve is less steep than Ganymede's expected core adiabat (i.e. $(\text{d}T_{\text{melt}}/\text{d}P) < (\text{d}T/\text{d}P)_{\text{ad}}$), and for even larger sulfur concentrations the melting temperature can decrease with increasing pressure (i.e. $(\text{d}T_{\text{melt}}/\text{d}P) < 0.0$; Fei et al., 1997). These observations imply that, for sulfur concentrations greater than 3%, Fe will first condense at Ganymede's core–mantle boundary (i.e. at the top of the liquid core), rather than at the inner-core/outer-core boundary as occurs on Earth (Kuang and Stevenson, 1996; McKinnon, 1996; Hauck et al., 2006). The relatively dense Fe condensed at the top of the liquid core is buoyantly unstable and will sink downward to form an inner core, releasing gravitational energy (Hauck et al., 2006). Hauck et al. (2006) have argued that such compositional convection is sufficient to drive Ganymede's dynamo. However, because condensation of Fe occurs at the core–mantle boundary rather than deep in the core, the latent heat released by Fe condensation might not contribute to the convection that drives the dynamo because this heat is immediately removed from the core to the cooler mantle above. The removal of the latent heating term from Eq. (4) severely limits the ability of compositional convection to power the dynamo. This is especially true in Ganymede's small core where the gravitational energy release is relatively small (see Section 2.1.2). Furthermore, while the gravitational energy re-

Author's personal copy

Table 1
Symbols and parameter values

b	Length of burger vector	0.5	nm
$c_{p,I}$	Ice specific heat	1800	$\mathrm{J\,kg^{-1}\,K^{-1}}$
$c_{p,w}$	Water specific heat	4218	$\mathrm{J\,kg^{-1}\,K^{-1}}$
$c_{p,\mathrm{sil}}$	Silicate specific heat	1149	$\mathrm{J\,kg^{-1}\,K^{-1}}$
$c_{p,c}$	Core specific heat	800	$\mathrm{J\,kg^{-1}\,K^{-1}}$
$\mathcal{C}$	Constant for temp. dep. ice thermal conductivity	651	$\mathrm{W\,m^{-1}}$
g	Surface gravity	1.4	$\mathrm{m\,s^{-2}}$
g_c	Core/mantle boundary gravity	1.3	$\mathrm{m\,s^{-2}}$
G	Gravitational constant	6.672×10^{-11}	$\mathrm{N\,m^2\,kg^{-2}}$
k_{sil}	Silicate thermal conductivity	3.5	$\mathrm{W\,m^{-1}\,K^{-1}}$
k_c	Core thermal conductivity	32	$\mathrm{W\,m^{-1}\,K^{-1}}$
L_w	Latent heat of water	3.33×10^5	$\mathrm{J\,kg^{-1}}$
L_{Fe}	Latent heat of iron	3×10^5	$\mathrm{J\,kg^{-1}}$
L_{sil}	Latent heat of silicates	6×10^5	$\mathrm{J\,kg^{-1}}$
P_{cmb}	Pressure at core/mantle boundary	7.0	GPa
R	Gas constant	8.314	$\mathrm{kJ\,mol^{-1}\,K^{-1}}$
R_g	Radius of Ganymede	2634	km
R_{sil}	Radius of silicates	1720	km
R_c	Radius of core	700	km
T_s	Surface temperature	100	K
T_o	FeS melting curve parameter	1880	K
T_{m1}	FeS melting curve parameter	1.36×10^{-11}	$\mathrm{K\,Pa^{-1}}$
T_{m2}	FeS melting curve parameter	-6.2×10^{-23}	$\mathrm{K\,Pa^{-2}}$
α_{ice}	Ice thermal expansivity	1.6×10^{-4}	$\mathrm{K^{-1}}$
α_{sil}	Silicate thermal expansivity	3×10^{-5}	$\mathrm{K^{-1}}$
α_c	Core thermal expansivity	1×10^{-4}	$\mathrm{K^{-1}}$
ϵ	Dynamo efficiency	0.05	–
η	Magnetic diffusivity	2	$\mathrm{m^2\,s^{-1}}$
μ	Shear modulus	80	GPa
$\mu_\circ$	Magnetic permeability	$4\pi \times 10^{-7}$	$\mathrm{N\,A^{-1}}$
ρ_I	Average ice density	1200	$\mathrm{Kg\,m^{-3}}$
ρ_w	Water density	1000	$\mathrm{Kg\,m^{-3}}$
ρ_{sil}	Silicate density	3300	$\mathrm{Kg\,m^{-3}}$
ρ_c	Average core density	6500	$\mathrm{Kg\,m^{-3}}$
ρ_{ic}	Inner core density	7020	$\mathrm{Kg\,m^{-3}}$
ρ_s	FeS density	5333	$\mathrm{Kg\,m^{-3}}$
ς	Non-dimensional slope of the FeS melting curve	2.09	–

leased through iron precipitation is identical to that of Earth-like "bottom-up" core formation, it is unclear whether the simple settling of iron grains can induce sufficient turbulence to generate a dynamo. Finally, we note that condensation of Fe grains at the core mantle boundary creates a stably stratified compositional gradient within the outer core that inhibits convection.

Due to the difficulties in maintaining Ganymede's magnetic field by long-lived-thermal or compositional convection associated only with the decline in radiogenic heating, Stevenson (1996) and Showman et al. (1997) suggested that a period of tidal heating in Ganymede's past may have enabled generation of the present-day field. The Galilean satellites Io, Europa, and Ganymede currently reside in a Laplace resonance. In this configuration there exists both 2:1 mean motion resonances between the satellite pairs Io and Europa, and Europa and Ganymede, as well as a 1:1 commensurability between the drift rates of the conjunctions of the satellite pairs ($\omega_1 = \omega_2$, where $\omega_1 = 2n_2 - n_1$ and $\omega_2 = 2n_3 - n_2$ and n_1, n_2, and n_3 are the mean motions of Io, Europa, and Ganymede respectively). These resonances excite the eccentricity of both Io and Europa, and the resulting tidal heat strongly influences their thermal histories (e.g. Yoder, 1979; Ojakangas and Stevenson, 1986; Fischer and Spohn, 1990; Hussman and Spohn, 2004). The Laplace resonance does not, however, force Ganymede's eccentricity, and thus negligible tidal heating currently occurs there.

Despite the present lack of tidal forcing of Ganymede's orbit, excitation of the satellite's eccentricity sufficient to drive thermal activity may have occurred in the past (Greenberg, 1987; Tittemore, 1990; Malhotra, 1991; Showman and Malhotra, 1997; Peale and Lee, 2002). Malhotra (1991) and Showman and Malhotra (1997) investigated one of the more plausible scenarios, which identified additional evolutionary pathways into the Laplace resonance to that described by Yoder and Peale (1981). In some of these pathways Io, Europa, and Ganymede pass through one or more Laplace-like resonance ($\omega_1/\omega_2 = 1/2, 2, 3/2$, etc.) before being captured into the Laplace resonance ($\omega_1/\omega_2 = 1$). Unlike the Laplace resonance, several of these resonances can strongly force Ganymede's eccentricity with the resulting tidal heating modifying the satellite's thermal history (Showman et al., 1997). Showman et al. (1997) investigated the potential for thermal runaway in Ganymede's ice shell during such resonance passage, but they did not explore the effect of resonance passage on Ganymede's silicate mantle and metallic core in detail.

In this paper, we first establish the conditions required to produce Ganymede's present-day core dynamo during its secular thermal evolution. We show that magnetic field production requires a very restrictive set of initial conditions be met, some of which may be incompatible with realistic models of the satellite. We then test the hypothesis that resonance passage may have broadened the range of conditions under which magnetic field generation is possible by reinvigorating the core dynamo: dissipation of tidal energy within Ganymede's silicate mantle drives a thermal runaway that prevents the metallic core from cooling. Such thermal runaways result from the complex feedback between temperature, viscosity, and tidal dissipation (Showman et al., 1997). Once the system escapes the resonance, tidal dissipation ends and the silicate mantle and metallic core cool rapidly until reaching a new quasiequilibrium with radiogenic heat production in the mantle. Dynamo action occurs during this period of rapid cooling and high core power output. Wienbruch and Spohn (1995) explored a similar scenario for Io (without the resonance escape) and suggested that tidal heating may prevent dynamo action there. The apparent absence of a strong magnetic field at Io

Author's personal copy

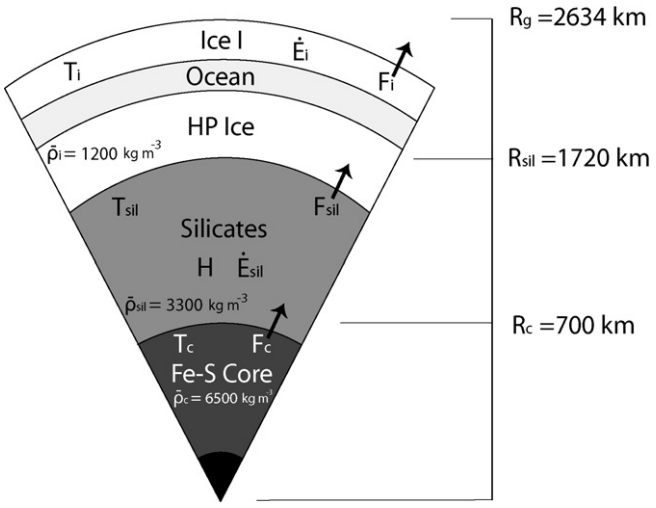

Fig. 1. Assumed physical and thermal structure for Ganymede. The model allows both inner core formation and ocean formation as illustrated, though these layers are not included in the initial condition. Symbols correspond to those used in the text and average densities are shown. Other relevant parameters are provided in Table 1.

(Kivelson et al., 2001) lends some credence to this scenario. However, even the strongest Laplace-like resonance produces approximately two orders of magnitude less tidal dissipation in Ganymede than is currently observed at Io (Showman and Malhotra, 1997; Veeder et al., 1994). Thus, elucidating the conditions (if any) under which tidal heating in Ganymede's silicates might assist present-day dynamo action in Ganymede's core is essential to understanding why the satellite has a magnetic field. Because an analytical description of the satellite's orbital evolution through the Laplace-like resonances is difficult to obtain, and because the magnitude of the tidal dissipation in the silicate layer depends critically on the details of both Ganymede's composition and its thermal evolution (see Sections 3.2.1, 3.2.3, and 3.2.4), we chose to model the coupled orbital-thermal evolution of Ganymede numerically. In doing so, we provide a robust test of the hypothesis that Ganymede's magnetic field is enabled by a past resonance passage.

2. Methods

We investigate the thermal history of Ganymede in an effort to understand the conditions required to produce Ganymede's magnetic field. In addition, we assess the role that resonance passage may have played in enabling a magnetic dynamo. To do this we couple a three-layer one-dimensional thermal model of Ganymede's ice shell, silicate mantle, and metallic core (Section 2.1 and Fig. 1) to the orbital model of Malhotra (1991) (Section 2.2). Coupling between the orbital and thermal models occurs via tidal dissipation, which depends upon both the thermal structure and orbital evolution of the satellite. We calculate tidal heating with the dissipation model of Tobie et al. (2005) (Section 2.3), which permits determination of the tidal dissipation in each model layer. The three models are described below.

2.1. The thermal model

2.1.1. Energy balance in the ice shell and silicate mantle

The thermal evolution of Ganymede is controlled by how energy is transferred between the three layers of the model. We solve for the energy balance in each layer as a function of time using a 4th order Runga–Kutta algorithm. The energy balance in the ice shell and silicate mantle are respectively given by

$$4\pi R_{\rm sil}^2 F_{\rm sil} + \dot{E}_I = 4\pi R_g^2 F_I + \frac{4}{3}\left(R_g^3 - R_{\rm sil}^3\right)\rho_I c_{p,I}\frac{{\rm d}T_I}{{\rm d}t}, \quad (5)$$

$$\frac{4}{3}\pi\left(R_{\rm sil}^3 - R_c^3\right)\rho_{\rm sil}H + 4\pi R_c^2 F_c + \dot{E}_{\rm sil} = 4\pi R_{\rm sil}^2 F_{\rm sil} + \frac{4}{3}\pi\left(R_{\rm sil}^3 - R_c^3\right)\rho_{\rm sil}c_{p,\rm sil}\frac{{\rm d}T_{\rm sil}}{{\rm d}t}, \quad (6)$$

where R_g, $R_{\rm sil}$, and R_c are the radius of Ganymede, the silicate mantle, and the metallic core respectively; F_I, $F_{\rm sil}$, and F_c are the heat flux out of the ice shell, silicate mantle, and metallic core respectively; $\dot{E}_I$, $\dot{E}_{\rm sil}$, ρ_I, $\rho_{\rm sil}$, $c_{p,I}$, $c_{p,\rm sil}$, T_I, and $T_{\rm sil}$ are the tidal heating rates, average densities, specific heats, and mean temperatures of the ice shell (I) and silicate mantle (sil) respectively; and t is time. H is the radiogenic heating rate per unit mass calculated after Kirk and Stevenson (1987), which includes contributions from the decay of K^{40}, Th^{232}, U^{235}, and U^{238}. The energy balance in the core is described in Section 2.1.2. Physical parameters used in the ice, silicates, and core are provided in Table 1. For simplicity, we do not treat the thermal balance in Ganymede's high pressure ice layers or liquid water, assuming that they are not a barrier to heat transfer. Instead, we assume heat transport through the whole H_2O layer is determined only by the efficiency of heat transfer through the outer ice shell.

If the temperature of the ice shell exceeds the minimum melting temperature of ice (251 K), ocean formation occurs. Following Showman et al. (1997), we modify the energy balance of the ice shell (Eq. (5)) to account for both the latent heat removed by melting and the larger specific heat of liquid water. These two effects act to buffer changes in the ice shell temperature. We determine the depth of the ocean by equating an ocean adiabat to the melting curve for ice and solving for the depth of intersection assuming hydrostatic equilibrium. We account for the changes in the melting curve as melting proceeds through high pressure ice layers (III, V, and VI), as well as the increase in water's coefficient of thermal expansion with depth. Further details of ocean formation are described in Bland et al. (submitted for publication). The latent heat of melting, density, and specific heat of water are given in Table 1.

Heat is transferred through the ice shell and silicate mantle either by conduction or convection. We assume a constant thermal conductivity for the silicate layer. The conducted heat flux thus has the form

$$F_{\rm cond} = k\frac{\Delta T}{\mathcal{L}}, \quad (7)$$

where ΔT is the temperature drop across the silicate layer, k is the thermal conductivity, and $\mathcal{L}$ is the thickness of the layer. In the ice shell, we assume a temperature dependent thermal conductivity so the conducted flux has the form

$$F_{\rm cond} = \frac{\mathcal{C}}{\mathcal{L}}\ln\left(T/T_s\right), \quad (8)$$

where T_s is the surface temperature, and $\mathcal{C} = 651$ W m^{-1} is a constant defined by the temperature dependent thermal conductivity $k_I = \mathcal{C}/T_I$ (Petrenko and Whitworth, 1999).

We parameterize stagnant lid convection using the scaling relations of Solomatov and Moresi (2000). The convective heat flux is given by

$$F_{\rm conv} = Nu\frac{k\Delta T}{\mathcal{L}}, \quad (9)$$

where ΔT is the temperature drop across the layer, k is the thermal conductivity (temperature dependent for ice, as shown above), and Nu is the Nusselt number with the form

$$Nu = aRa^{\beta}\Theta^{-\gamma}, \quad (10)$$

where a, β, and γ are experimentally and theoretically derived constants (Solomatov and Moresi, 2000), Ra is the Rayleigh num-

Author's personal copy

ber (defined below) and Θ is the logarithm of the viscosity contrast across the convecting layer. Ignoring the small dependence on pressure, Θ is given by

$$\Theta = \frac{\Delta T Q}{RT^2}, \tag{11}$$

where Q is the rheological activation energy, R is the gas constant, and T is the temperature.

We utilize a power-law rheology in the silicate mantle and ice shell. The stress strain-rate relation in the silicates is given by (Karato and Wu, 1993)

$$\dot{\varepsilon} = A_{\text{sil}}\left(\frac{\tau}{\mu}\right)^n\left(\frac{b}{d}\right)^p \exp\left[-Q_{\text{sil}}/(RT)\right], \tag{12}$$

where $\dot{\varepsilon}$ is the strain rate, τ is the shear stress, μ is the shear modulus (~80 GPa; Karato and Wu, 1993), n is the power-law exponent, b is the length of the burgers vector (~0.5 nm; Karato and Wu, 1993), d is the grain size (nominally 1 mm), p is the grain size exponent, and A_{sil} is a rheological constant. We have ignored the small dependence of $\dot{\varepsilon}$ on pressure since it is poorly constrained (Karato and Wu, 1993) and within the uncertainty imposed by our lack of knowledge of grain size and silicate composition. Rheologically, Ganymede's mantle most likely consists of dry olivine, consistent with a highly differentiated body (Kuskov and Kronrod, 2001; Sohl et al., 2002), but for completeness we investigate both dry and wet rheologies. In the temperature and stress regimes examined here, either dislocation creep or diffusion creep can dominate the silicate flow depending on the choice of grain size. To determine which mechanism dominates we calculate the strain rate associated with each flow mechanism at every thermal timestep. The mechanism with the highest strain rate will dominate the convection.

For the ice shell we assume a power-law rheology with the form

$$\dot{\varepsilon} = A_{\text{ice}}\tau^n(1/d)^p \exp\left[-Q_{\text{ice}}/(RT)\right], \tag{13}$$

where the variables are defined as above. As with the silicate rheology, one of two viable rheological mechanisms, diffusion creep or grain-boundary-sliding, dominates depending on the grain size. As the temperature in the ice shell changes we again allow transitions to occur between the two rheological regimes by comparing the strain rates produced by the two flow mechanisms at each timestep. All rheological parameters are shown in Table 2.

Calculation of Nu (Eq. (10)) depends upon the Rayleigh number, which for a power-law fluid is given by

$$Ra = \frac{\alpha g \rho \Delta T d^{(n+2)/n}}{c^{1/n}\kappa^{1/n}\exp[Q/(nRT)]}, \tag{14}$$

where $\kappa = k/\rho c_p$ is the thermal diffusivity, and c is a function of rheological parameters and is given by $c = \mu^n(d/b)^p/A_{\text{sil}}$ for a silicate rheology, and $c = d^p/A_{\text{ice}}$ for an ice rheology. The parameters a, β, and γ, used in the scaling of the convective Nusselt number (Eq. (10)) depend on the power-law exponent of the rheology that dominates each layer (Solomatov and Moresi, 2000). We self-consistently modify these values when (or if) the dominant rheology changes during a simulation. For simplicity we assume only scaling laws derived for time-dependent (vigorous) convection. The convective scaling parameters are shown in Table 3.

Table 3
Convective scaling $Nu = aRa^{\beta}\Theta^{-\gamma}$

Power-law exponent[a]	a	β	γ
$n = 3$	0.97	0.6	1.6
$n = 2$	0.76	0.5	1.5
$n = 1$	0.53	0.333	1.333

[a] Refers to the rheological exponent (Eqs. (12) and (13)). From Solomatov and Moresi (2000).

Using the rheological laws described, we define an effective viscosity for the ice and silicates with the form

$$\eta_e = \frac{c}{\tau^{n-1}}\exp\left[Q/(RT)\right], \tag{15}$$

where all parameters are defined above. The effective viscosity depends upon the convective stress in each layer, which we calculate from the convective scaling laws as (Solomatov and Moresi, 2000)

$$\tau = 0.027\alpha\rho g\Delta T_{rh}\delta_{rh}, \tag{16}$$

where the value 0.027 is a numerically derived constant, $\Delta T_{rh} = 1.2(n+1)\theta^{-1}\Delta T$ (Solomatov and Moresi, 2000) is the temperature drop across the convective sublayer, and $\delta_{rh} \approx \mathcal{L}/Nu$ is the thickness of the convective sublayer beneath the stagnant lid (Solomatov, 1995).

To determine whether each layer is conducting or convecting we calculate the critical Rayleigh number (Ra_{crit}) for convection in a power law fluid at each timestep. Ra_{crit} is given by (Solomatov, 1995; Solomatov and Barr, 2006)

$$Ra_{\text{crit}} = Ra_n\Theta^{2(n+1)/n}\left[\frac{e}{4(n+1)}\right]^{2(n+1)/n}, \tag{17}$$

where

$$Ra_n = 1568^{1/n}20^{(n-1)/n}, \tag{18}$$

and e is the base of the natural logarithm. Convection occurs if Ra is greater than Ra_{crit}. In reality, for a power-law fluid the critical Rayleigh number is also sensitive to the wavelength and amplitude of the temperature perturbation that initiates convection (Solomatov and Barr, 2007). However, for simplicity we assume that once convection is possible (i.e. $Ra \geqslant Ra_{\text{crit}}$) convection will occur.

2.1.2. The core model

Cooling, offset by the energy released by inner core formation, dominates the thermodynamics of Ganymede's core. The core's energy balance can be described as

$$(E_G + L_{Fe})\frac{dm_{ic}}{dt} = 4\pi R_c^2 F_c + \frac{4}{3}\pi R_c^3\rho_c c_{p,c}\frac{dT_c}{dt}, \tag{19}$$

Table 2
Rheological parameters

	Creep regime	A	n	p	Q	Reference
Silicates						
	Dislocation creep (dry)	3.5×10^{22} s^{-1}	3.5	0	540 kJ mol^{-1}	Karato and Wu (1993)
	Diffusion creep (dry)	8.7×10^{15} s^{-1}	1.0	2.5	300 kJ mol^{-1}	Karato and Wu (1993)
	Dislocation creep (wet)	2.0×10^{18} s^{-1}	3.0	0	430 kJ mol^{-1}	Karato and Wu (1993)
	Diffusion creep (wet)	5.3×10^{15} s^{-1}	1.0	2.5	240 kJ mol^{-1}	Karato and Wu (1993)
Ice I						
	Diffusion creep	1.2×10^{-10} Pa^{-n} m^p s^{-1}	1.0	2.0	59.4 kJ mol^{-1}	Goldsby and Kohlstedt (2001)
	GBS	6.2×10^{-14} Pa^{-n} m^p s^{-1}	1.8	1.4	49.0 kJ mol^{-1}	Goldsby and Kohlstedt (2001)

Rheological constant 'A' must be multiplied by a factor of $3^{(n+1)/2}$ (Ranalli, 1995).

Author's personal copy

where L_{Fe} is the latent heat released by condensation of iron, E_G is the gravitational energy release per unit mass associated with iron condensation (see below), m_{ic} is the mass of the inner core, ρ_c is the density of the core, $c_{p,c}$ is the specific heat of the core, and F_c is heat flux out of the core. In the absence of inner core formation dm_{ic}/dt is zero. The heat flux out of the core F_c is controlled by energy transfer across the core mantle boundary (CMB), which must occur conductively. The heat flux is

$$F_c = k_{\rm sil}\frac{T_{\rm cmb} - T_{\rm sil}}{\delta_{\rm BL}}, \tag{20}$$

where $\delta_{\rm BL} = \mathcal{L}(Ra_{\rm crit}/Ra)^{\beta}$ is the thickness of the thermal boundary layer in the silicate mantle, and $\mathcal{L}$ is the thickness of the silicate mantle. Because the thermodynamics of the core are slave to those of the silicate mantle above, a more detailed parametrization of convective or conductive heat transfer within the core is not warranted. Equation (20) is an approximation to the true heat flux across the core–mantle boundary, which requires that the silicate mantle is hot and vigorously convecting (if the silicate mantle is cool, $\delta_{\rm BL}$ is large and the flux out of the core will be negligible in spite of large potential differences in $T_{\rm sil}$ and $T_{\rm cmb}$). This requirement is met in all of the simulations described below. Furthermore, radiogenic heating within the silicate layer will modify the thickness of the bottom boundary layer compared to that determined from boundary stability analysis (used above). Finally, we note that a rigorous formulation of the heat flux out of the core must correct for the sphericity of the layer (cf. Reese et al., 2005). For simplicity we have neglected the effects of curvature as we expect these effects to be less important than other model uncertainties.

When the core temperature drops below the melting point of the Fe–FeS system, condensation of Fe will occur and an inner core will form. We model inner core formation following the approach of Stevenson et al. (1983) and we refer readers there for a more detailed description of the model. We assume an adiabatic temperature profile for the core with the form

$$T_c = T_{\rm cmb}\exp\left[\frac{\alpha_c(P(r) - P_{\rm cmb})}{\rho_c c_{p,c}}\right], \tag{21}$$

where $T_{\rm cmb}$ and $P_{\rm cmb}$ are the temperature and pressure (~7 GPa; Sohl et al., 2002) at the core–mantle boundary respectively, α_c is the coefficient of thermal expansion, and $P(r)$ is the pressure at depth r. The melting curve in the Fe–S system is given by

$$T_m = T_o\left[1 + T_{m1}P(r) + T_{m2}P(r)^2\right][1 - \varsigma\chi], \tag{22}$$

where T_o, T_{m1}, and T_{m2} are experimentally derived constants, and χ is the mass fraction of light elements. ς is the dimensionless slope of the Fe/FeS liquidus as a function of composition (Fei et al., 1997; Hauck et al., 2006). For simplicity we neglect the small pressure dependence of ς. All parameter values are given in Table 1. We calculate the radius of the inner core $R_{\rm inner}$ at each timestep by equating Eqs. (21) and (22) and solving for $P(r)$, the pressure of the top of the inner core. An inner core radius can be determined from $P(r)$ by assuming hydrostatic equilibrium.

The gravitational energy released by condensation of iron (E_G) is given by (Schubert et al., 1988)

$$E_G = \frac{2\pi G R_c^2 \chi_o \Delta\rho}{(1-\xi^3)^2}\left(\frac{\rho_{ic}}{\rho_s}\right)\left[\frac{1}{5}(1-\xi^5) - \frac{\xi^2}{3}(1-\xi^3)\right], \tag{23}$$

where G is the gravitational constant, χ_o is the initial sulfur concentration, $\Delta\rho$ is the density difference between the light element and iron, ρ_{ic} is the density of the inner core, ρ_s is the density of sulfur, and $\xi = R_{\rm inner}/R_c$. For $R_c \sim 700$ km, and an initial sulfur concentration of 10%, typical values of E_G are 10^4 J kg^{-1}, an order of magnitude less than the latent heat released by iron condensation. For an initial sulfur concentration of 1% the gravitational energy is an additional order of magnitude lower. Thus, during inner core growth the release of latent heat dominates the core energy balance.

2.1.3. Initial thermal conditions

The model described above implicitly assumes that the satellite differentiated shortly after accretion (i.e. before our simulated tidal evolution begins), and the effects of such differentiation are not included in the model. Thus $t = 0$ should be considered the time after differentiation occurred. We assume that differentiation occurred quickly enough that long-lived radiogenic isotopes did not undergo significant decay [i.e. the timescale for accretion of ~10^3 yrs (Canup and Ward, 2002) is much shorter than typical radiogenic half life of ~10^9 yrs]. We therefore assume that Ganymede possess its full complement of radiogenic isotopes when the simulations begin.

We assume that the silicate mantle and metallic core begin hot. Starting the simulations with cooler temperatures leads to an initial period of rapid warming as the silicate temperatures come into quasi-equilibrium with radiogenic heating. This initial period of heating does not influence the later temperature evolution of the satellite and it appears more realistic to simply initialize the simulations with high temperatures. Additionally, we initialize our simulations with core temperatures that are slightly overheated relative to the silicate mantle. In reality, the temperature of Ganymede's core shortly after its formation likely depends on the details of how core formation occurs in icy satellites, a topic beyond the scope of the present investigation. Thus, we simply assume reasonable values and assess the sensitivity of our results to those assumptions (discussed below).

2.2. The orbital model

We use the orbital model of Malhotra (1991) to simulate the tidally driven evolution of the Galilean satellites into the Laplace resonance. The model is a generalization of the evolutionary scenario described by Yoder and Peale (1981) that allows a more complete dynamical investigation of the orbital history of the satellites. This includes capture into one or more Laplace-like resonance, which cannot be explored by analytical representations of the tidal evolution (e.g. Ojakangas and Stevenson, 1986; Fischer and Spohn, 1990; Hussman and Spohn, 2004). The model includes perturbations due to Jupiter's gravity field, mutual perturbations between the satellites Io, Europa, and Ganymede, and secular perturbations due to Callisto. Forward integration allows determination of the eccentricity, semi-major axis, mean longitude, and longitude of periapse of each satellite. The effects of orbital inclinations are neglected. See Malhotra (1991) and Showman and Malhotra (1997) for further details.

2.3. Tidal heating

We use the model of Tobie et al. (2005) to calculate the radial distribution of tidal heating per unit volume within Ganymede. The derivation is not repeated here but see Tobie et al. (2005). The resulting expression has the form

$$h_{\rm tide} = -\frac{21}{10}\frac{n_3^5 R_g^4 e^2}{r^2} H_\mu \,{\rm Im}\{\mu\}, \tag{24}$$

where n_3 is Ganymede's mean motion, e is the eccentricity, r is the radius from the center of mass, and H_μ and Im$\{\mu\}$ are the radial sensitivity to the shear modulus and imaginary part of the complex shear modulus, respectively. The H_μ parameter quantifies the viscoelastic response of each internal layer to tidal forcing. It is calculated assuming a Maxwell rheology and depends on the radial

Author's personal copy

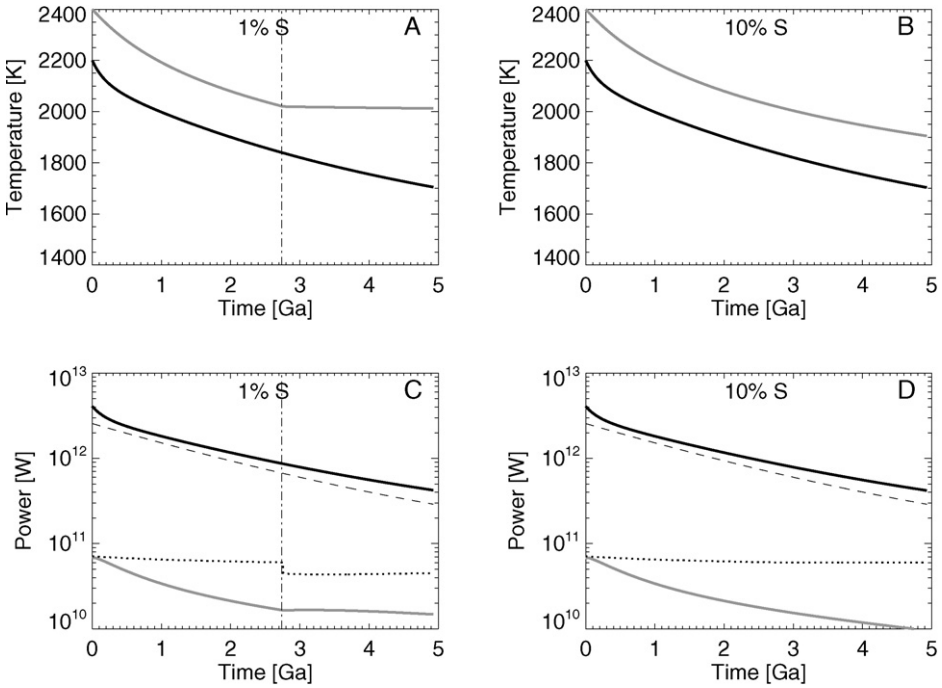

Fig. 2. Thermal history of Ganymede's core and silicate mantle assuming a dry silicate rheology with a 1 mm grain size. (A) Temperature of the silicate mantle (black line) and metallic core (gray line) as a function of time for a simulation with a core sulfur mass fraction of 1%. (B) Same as in (A) but for a simulation with a core sulfur mass fraction of 10%. (C) Power output from the silicate mantle (black line) and metallic core (gray line) for a simulation with a core sulfur mass fraction of 1%. The power required to drive Ganymede's core dynamo is indicated by a dotted line. For reference, the radiogenic power is shown as a dashed line. (D) Same as in (C) but for a simulation with a core sulfur mass fraction of 10%. In each panel the onset of inner core formation is indicated by a vertical dot–dash line.

structure of the satellite and the radial functions of displacement, stress, and potential (see Tobie et al., 2005, for more detail).

For the purposes of the tidal heating calculation we further subdivide the three layer structure of our thermal model (ice, silicate, core) into a metallic core, silicate layer, silicate stagnant lid, high-pressure ice layer, ice I layer, and ice stagnant lid. If ocean formation occurs a liquid ocean layer is added between the high-pressure ice and ice I layers. The thickness of the ocean and ice layers are updated at each timestep to coincide with values derived from the thermal model. The density, bulk modulus, and shear modulus of each of these layers is assumed spatially and temporally constant throughout the layer, while the viscosities are updated at each timestep. Because negligible tidal dissipation occurs in the stagnant lids of the ice shell and silicate mantle, tidal dissipation is averaged over only the actively convecting region of each layer. We also assume that no tidal dissipation occurs within the metallic core or ocean (if present).

In addition to the tidal dissipation, the model calculates the global value of k_2/Q_3, where k_2 is the 2nd degree tidal love number, and Q_3 is Ganymede's tidal dissipation factor, at each timestep for use in the orbital dynamics algorithms.

3. Model results

3.1. Producing Ganymede's magnetic field

The thermal history of Ganymede was assessed to determine conditions under which a present-day magnetic field can be produced by a thermally or compositionally driven dynamo operating in Ganymede's core. These simulation do not include tidal dissipation and are consistent with a primordial origin for the Laplace resonance, passage through Laplace-like resonances that do not pump Ganymede's eccentricity, or tidal evolution directly into the Laplace resonance (i.e. avoiding the Laplace-like resonances). Each simulation was initialized with a hot core (2400 K), hot mantle (2200 K), and cold ice shell (200 K). The grain size of the silicates and ice was 1 mm, and we evaluated the effects of both a wet and dry olivine rheology for the mantle (Table 2). Additionally, we investigated two end member core compositions: a sulfur mass fraction of 1%, placing it in the "Earth-like" bottom-up regime for inner core formation, and a sulfur mass fraction of 10%, placing it in the "iron snow" top-down regime of inner core formation.

Fig. 2 shows the thermal evolution of Ganymede assuming a dry olivine mantle rheology for the two end member core compositions. Silicate and core temperatures (Figs. 2A and 2B) are controlled by the quasiequilibrium between radiogenic heat production and convective cooling and are maintained between 2200 and 1700 K throughout the simulation. These high temperatures suggest melting should occur within Ganymede's mantle. The effects of partial melting are described in Section 3.2.4. Our calculated temperatures are roughly consistent with previous modeling by Hauck et al. (2006) whose somewhat lower temperatures can be attributed to the use of a wet olivine rheology (see below). Freeman (2006) calculated significantly lower temperatures for Ganymede's silicate mantle and ice shell. Their lower temperatures likely result from the use of different parameterizations for the ice and silicate viscosity and different scaling laws for the convective heat flux.

For both core compositions, the power output of the core (solid gray line in Figs. 2C and 2D) is initially equal to the power required to drive the dynamo (Eq. (4), dotted line in Figs. 2C and 2D) but immediately drops below the requirement. A dry mantle rheology therefore does not permit a magnetic field early (or late, see below) in Ganymede's history. In the simulation with a sulfur mass fraction of 1% in the core (Figs. 2A and 2C), inner core formation (indicated by the vertical dot–dash line) begins after 2.75 Ga, significantly reducing the cooling rate of the core. The onset of chemical convection reduces the power requirement on the dynamo but, because of slow inner core growth, the magnitude of the reduction is insufficient to permit the core power output to exceed the dynamo requirement (Fig. 2C). In the simulation with a core sulfur

Author's personal copy

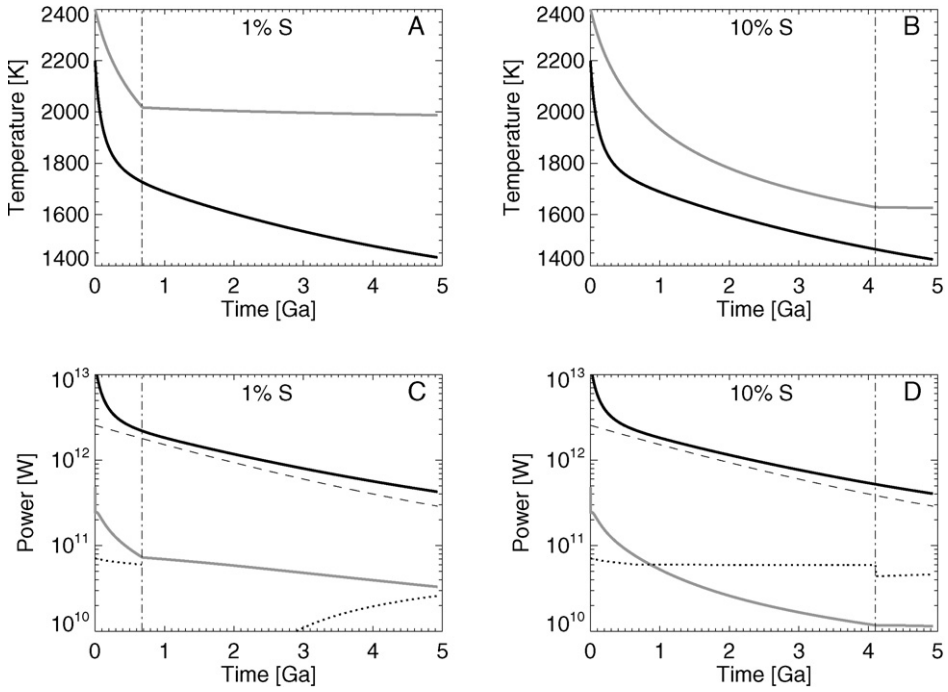

Fig. 3. As in Fig. 2 but for a wet silicate rheology with a 1 mm grain size.

mass fraction of 10% (Figs. 2B and 2D), temperatures never drop below the core melting temperature (which is reduced by the increased sulfur concentration) and compositional convection never occurs. We therefore conclude that present-day magnetic field production is not possible if Ganymede's mantle cools slowly (i.e. has a rheology similar to dry olivine).

Ganymede's thermal history is substantially different if we assume the silicate mantle behaves like wet olivine (Fig. 3). Temperatures decrease rapidly relative to the simulations with a dry olivine rheology and are generally consistent with the temperatures calculated by Hauck et al. (2006). Temperatures are again higher than those of Freeman (2006), as discussed above. In the simulation with a core sulfur mass fraction of 1% (Figs. 3A and 3C), the power output of the rapidly cooling core initially greatly exceeds the power requirement for the dynamo, suggesting that a magnetic field driven solely by thermal convection may have existed early in Ganymede's history. Inner core formation begins at 0.7 Ga, at which point further cooling of the metallic core is strongly reduced by the release of latent heat and gravitational energy. The chemical energy released during inner core formation is sufficient to significantly reduce the power requirements on the dynamo, which initially drops to near zero. As the rate of core cooling decreases with time, the rate of inner core formation slows and the additional power needed for the dynamo begins to increase. Despite this, the power output of the core exceeds the power required to drive the dynamo throughout the simulation, suggesting that production of a present-day magnetic field is feasible under these simulated conditions.

A different story emerges in the simulation with a core sulfur mass fraction of 10% (Figs. 3B and 3D). Like the simulation with a 1% sulfur core composition, the core power output initially exceeds the dynamo power requirement, suggesting a thermally driven dynamo existed early in Ganymede's history. The greater sulfur concentration in the core lowers the core melting temperature and delays inner core formation until 4.1 Ga (note that the timing of inner core formation, which depends on the assumed initial core temperature, does not affect the results described here). Unlike the simulation described above however, the onset of chemical convection does not substantially decrease the dynamo power requirement. In the "iron snow" regime the latent heat released by iron condensation at the top of the core is immediately removed to the mantle above and is not available to power the dynamo. We therefore neglect the latent heating term in Eq. (4) when evaluating the power required to drive the dynamo. The effect of not including the latent heating term can clearly be seen by comparing panel C and D of Fig. 3. When the latent heat is included (low-S simulation, bottom-up inner core formation, panel C) the power requirement on the dynamo is greatly reduced once inner core formation begins and the core power output exceeds the requirement. When the latent heat is not available (high-S simulation, top-down inner core formation, panel D) the reduction in the dynamo power requirement (now due to gravitational energy release alone) is much smaller and the core power output falls short of driving a dynamo. Therefore, the high sulfur (10%) simulation does not predict magnetic field production during the current epoch.

These simulations illustrate that the production of Ganymede's current magnetic field during secular cooling of the satellite is feasible, but only for a select set of circumstances. Ganymede's core must contain less than ∼3% sulfur by mass. Core formation will then occur in an Earth-like regime in which latent heat is released deep in the core. With greater amounts of sulfur, Fe condensation occurs at the top of the core and the released latent heat is not available to drive the core dynamo. Gravitational energy alone cannot maintain Ganymede's dynamo and magnetic field production does not occur. We note that sulfur concentrations greater than the FeS eutectic (∼21%) may also permit condensation of FeS deep within Ganymede's core (McKinnon, 1996; Hauck et al., 2006). Such high sulfur concentrations are not investigated here, but they remain a viable possibility for driving a dynamo by compositional convection.

Despite calculating similar thermal evolution histories for Ganymede, our results contrast with those of Hauck et al. (2006) who find that chemical convection can drive Ganymede's magnetic dynamo for a broad range of core compositions. The different criteria used by the two models makes a direct comparison difficult. Hauck et al. (2006) examine whether the buoyancy flux associated with condensation of Fe grains at the top of the core causes sufficient mixing to drive a dynamo. In contrast, we sidestep the

Author's personal copy

question of whether sufficient mixing of the outer core occurs during top-down inner core formation and instead simply determine whether there is sufficient energy to actually maintain a dynamo. Using this criterion, we find that a dynamo cannot be maintained during top-down inner core growth. Again, it is the removal of the latent heat at the top of the core that renders the core power insufficient. Note that if we had included the latent heating term in the high-S, top-down cases the reduction in the dynamo requirement would again be large and the core power output *would* exceed the requirement. A dynamo would then be expected for a broad range of core sulfur contents, consistent with the findings of Hauck et al. (2006). We believe, however, that the more restrictive requirements on magnetic field production suggested by our simulations are physically more realistic.

Given that our simulations suggest that the production of Ganymede's magnetic field places a strict requirement on the core sulfur composition it is useful to consider whether such compositions are cosmochemically plausible. The compositions of icy satellite mantles and cores are poorly constrained (see Schubert et al., 2004, for a review) and depend, in part, on poorly known processes such as the time-varying chemistry of the solar nebula (Pasek et al., 2005), the formation of satellites in the jovian subnebula (e.g. Hersant et al., 2004; Mousis and Alibert, 2006), and the differentiation and chemical history of the satellites (e.g. Lewis, 1982; McKinnon, 2006). Furthermore, structural models often come to contradictory conclusions. Kuskov and Kronrod (2001) argued that Ganymede's mantle has a composition similar to the L or LL chondrites and is depleted in iron with respect to solar values. If true, Ganymede's core is iron rich (Kuskov and Kronrod, 2001). These conclusions are supported by McKinnon and Desai (2003) who found that a subsolar iron composition may be required to simultaneously explain Ganymede's density and moment of inertia. In contrast, the three-layer structural models of Sohl et al. (2002) find a large range of plausible iron contents for Ganymede's mantle, leaving the core composition unconstrained. Alternatively, if Ganymede's interior is sufficiently oxidized, then Ganymede's core may be sulfur rich with a composition that falls on the FeS side of the Fe–FeS eutectic (Scott et al., 2002). Thus current cosmochemical models provide few constraints on the true sulfur content of Ganymede's core.

In addition to the requirement on the core composition, chemical convection is a sufficient source of energy only if the core can cool rapidly, requiring that Ganymede's mantle behaves rheologically like wet olivine. Alternatively, a dry rheology is feasible if the grain size of the silicates is very small (~100 μm). Finally, the low sulfur concentration in the core required to power the dynamo implies that the core formed hot, with temperatures exceeding the melting point of a low-sulfur core alloy (>2000 K). Unfortunately the conditions described above are not easily met. The fact that Ganymede possesses a metallic core argues for a dehydrated mantle composition and a dry silicate rheology (Kuskov and Kronrod, 2001; Sohl et al., 2002). Furthermore, differentiation of a sulfur poor core may require temperatures higher than can be achieved in Ganymede's mantle (Grasset et al., 2000). Given these difficulties, an investigation of alternative mechanisms for the production of Ganymede's magnetic field is warranted. We now consider whether a period of tidal dissipation in Ganymede's silicate mantle can extend the range of conditions needed for the generation of a core dynamo beyond those described above.

3.2. The influence of Ganymede's orbital evolution

To evaluate the magnitude of the tidal dissipation required to modify the thermal history of Ganymede's silicate mantle and metallic core and enable magnetic field production we simulated the Galilean satellites' evolution through the Laplace-like resonance that produces the strongest excitation of Ganymede's eccentricity ($\omega_1/\omega_2 = 2$, where again $\omega_1 = 2n_2 - n_1$ and $\omega_2 = 2n_3 - n_2$ and n_1, n_2, and n_3 are the mean motions of Io, Europa, and Ganymede respectively) (Showman and Malhotra, 1997). The relevance of other evolutionary pathways is discussed in Section 4. In the simulations described here we assume a constant value for Jupiter's tidal dissipation factor (Q_J) of 3×10^5, consistent with observational and theoretical constraints (see review by Peale, 1999). The effect of variations in Q_J are discussed in Section 3.2.2. We assume initial ratios of tidal dissipation factor (Q) to second degree tidal love number (k) for Europa and Io of 3260.9 and 300, respectively. These ratios yield reasonable Q values for the expected k of the satellites. The low Q/k ratio of Io is required for capture into the $\omega_1/\omega_2 = 2$ resonance. The range of Io's Q/k that permits capture into the $\omega_1/\omega_2 = 2$ resonance depends upon the initial values of ω_1 and ω_2 and we refer the reader to Showman and Malhotra (1997) for more detail. The initial ratio of Q/k for Ganymede as calculated from the tidal dissipation model is ~3000 for the simulations described below. With these parameters, the satellites enter the $\omega_1/\omega_2 = 2$ resonance at 0.5 Ga and remain locked in resonance until ~3.8 Ga, at which point we force the system out of resonance by temporarily increasing Io's Q/k value. Because Io's thermal evolution is not modeled here we manually change Io's Q/k, however, such changes are consistent with coupled orbital-thermal models of the satellite (e.g. Ojakangas and Stevenson, 1986). Tidal dissipation in Io and Europa are calculated after Malhotra (1991). Once the system has escape the $\omega_1/\omega_2 = 2$ resonance, it evolves naturally into the Laplace resonance (Fig. 4A). The eccentricity of Ganymede (e_3) increases significantly while in the Laplace-like resonance (Fig. 4B), reaching values as high as 0.011, ~10 times greater than the satellite's current eccentricity. The timing of capture into the $\omega_1/\omega_2 = 2$ resonance and the maximum eccentricity reached by Ganymede depend on the assumed value of Q_J, with lower values causing rapid orbital evolution and larger satellite eccentricities. The increase in Ganymede's eccentricity during resonance passage leads to the dissipation of tidal energy in Ganymede's ice shell and silicate mantle (Fig. 4C). Negligible dissipation occurs in either layer before the satellites enter the Laplace-like resonance. Once capture occurs however, tidal dissipation increases sharply leading to nearly 10^{12} W of dissipation in the ice shell (gray line), and 10^9 W of dissipation in the silicates (black line).

Fig. 5 shows the effect of tidal dissipation on the temperature structure of the satellite. Initial temperatures are identical to those used in Section 3.1. We use a dry olivine rheology in the silicates, and a grain size of 1 mm in both the ice and silicate layers. The temperatures in the ice shell rise steadily due to the combination of radiogenic heat from below and tidal dissipation in the ice shell itself (Fig. 5A). Once the ice reaches a temperature of 251 K, ocean formation begins and the temperature increase is buffered by melting. As melting proceeds the ice shell transitions to a thin conductive layer, ultimately limiting the temperature of the ice, which then remains constant throughout the resonance passage. The thickness of the remnant ice I shell is generally a few tens of kilometers. After the satellites escape the Laplace-like resonance, ice temperatures decrease slowly, again buffered by the release of latent heat during refreezing of the ocean. We discuss details of the thermal history of the ice shell further in a companion paper (Bland et al., submitted for publication).

Fig. 5B shows the temperature of the silicate mantle and core and Fig. 5C shows the cooling rate of the core over Solar System history. Core temperatures decline monotonically at a rate determined by the cooling silicate layer above. The high initial cooling rates permit early thermal convection in the core (note that thermal convection does not necessarily imply magnetic field production, see below); however, cooling rates decrease rapidly in the

Author's personal copy

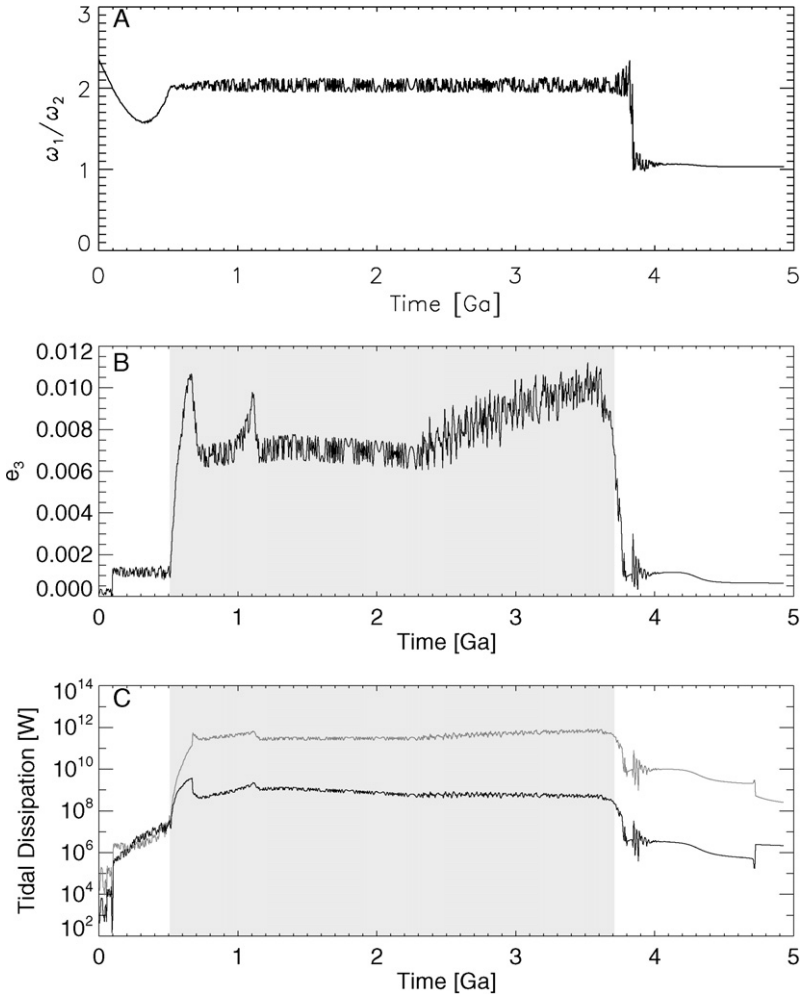

Fig. 4. A plausible orbital history for Ganymede. (A) Ratio between ω_1 and ω_2 ($\omega_1 = 2n_2 - n_1$ and $\omega_2 = 2n_3 - n_2$ where n_1, n_2, and n_3 are the mean motions of Io, Europa, and Ganymede respectively) as a function of time. The satellites enter the $\omega_1/\omega_2 = 2$ Laplace-like resonance after ~0.5 Ga and escape resonance at ~3.8 Ga. The system then evolves into the Laplace resonance in which $\omega_1/\omega_2 = 1$. (B) Ganymede's eccentricity (e_3) as a function of time. During the Laplace-like resonance passage e_3 reaches values of ~0.011, an order of magnitude larger than its current eccentricity. (C) Tidal dissipation in the ice shell (gray line) and silicate mantle (black line) as a function of time. Maximum tidal dissipation occurs during resonance passage and negligible dissipation occurs outside the resonance. The tidal dissipation in the ice shell is more than two orders of magnitude greater than that in the silicate mantle. Q_J is 3×10^5. The shaded region in (B) and (C) indicates the period of Laplace-like resonance passage shown in (A).

first 0.5 Ga. In the late stages of the simulations, the slow cooling of the silicates (Fig. 5B) prevents the core from cooling more rapidly than 30–50 $\mathrm{K\,Ga^{-1}}$. Like the previously described simulations with a dry olivine rheology, the high silicate temperatures prevent formation of an inner core, eliminating compositional convection as a potential driver for the dynamo.

Fig. 5D shows the power transported out of the ice shell (thin, solid line), silicate mantle (heavy, black line), and metallic core (gray line) respectively as a function of time. The power out of the silicates closely follows the radiogenic heat production, illustrating the insignificance of tidal dissipation in the silicates. The power out of the ice shell initially follows the radiogenic heat production but is eventually dominated by tidal dissipation in the ice shell, which exceeds radiogenic heat production after ~2.2 Ga. The core power is initially near the required dynamo power (again shown as a dotted line), but it decreases rapidly as the simulation progresses. While thermal convection in the core can occur early in the simulation (Fig. 5C), at no point during the simulation does the core power exceed the requirement for driving a dynamo. This result is independent of our assumptions about the ohmic dissipation. Therefore, the simulation described here does not predict a present-day magnetic field to be present at Ganymede.

Clearly, tidal dissipation does not affect the thermal history of Ganymede's mantle or core (Fig. 5 is nearly identical to Fig. 2), and thus cannot expand the range of conditions under which magnetic field production is achievable. This result is not surprising considering the tidal dissipation in the silicates (Fig. 4) is two orders of magnitude less than the radiogenic energy released. Despite the low magnitude of the tidal dissipation in this simulation, a number of mechanisms could increase the magnitude of the dissipation and these must be explored before the tidal heating mechanism for production of Ganymede's magnetic field can be rejected. All of the simulations described below assume a 10% sulfur mass fraction in the core; however, the conclusions apply to the full range of sulfur concentrations for which iron condenses at the top of the core.

3.2.1. Variation in the silicate rheology

Fundamentally, tidal dissipation in Ganymede's silicate mantle is low because of the high effective viscosity of the silicates. The magnitude of tidal deformation is maximized when the Maxwell time of the material ($T_M = \eta_e/\mu$, where η_e is the effective viscosity and μ is the shear modulus) is close to the tidal forcing period. Using the rheological parameters for dislocation creep in Table 2, a typical convective stress of 0.01 MPa, and a typical silicate temperature of 1800 K, T_M is ~10 yrs. In contrast, the

Author's personal copy

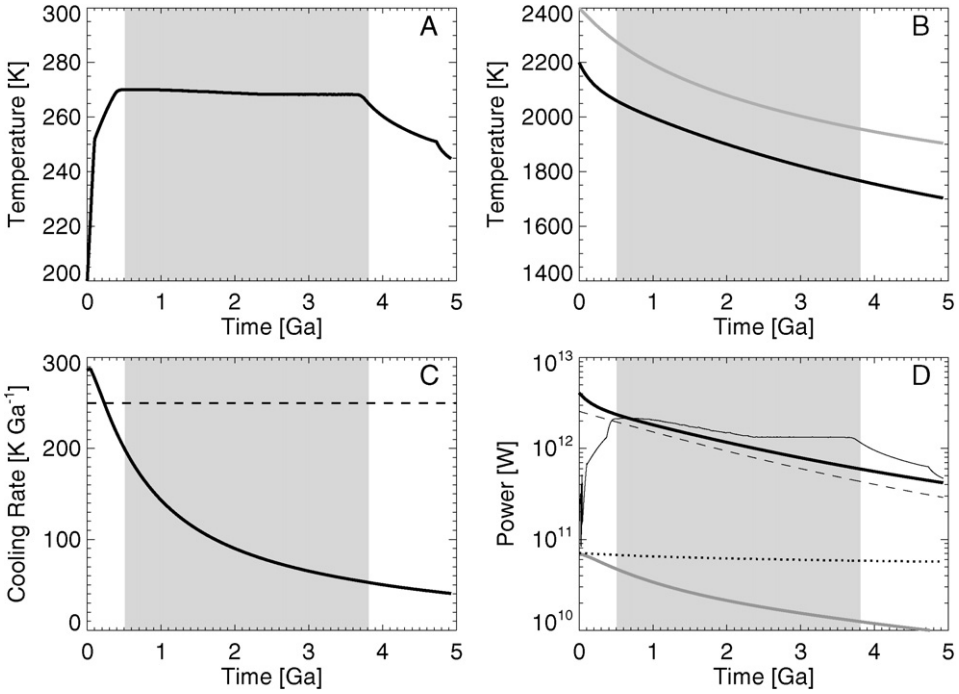

Fig. 5. The thermal history of Ganymede including Laplace-like resonance passage with $Q_J = 3 \times 10^5$ and assuming a dry silicate rheology with a 1 mm grain size. Initial temperatures are as in Figs. 2 and 3. (A) Temperatures in the ice shell. (B) Temperatures in the core (gray line) and silicate mantle (black line). (C) The core cooling rate. The thin dashed line indicates the cooling rate required for thermal convection to occur. (D) Power out of the core (gray line), silicate mantle (heavy black line), and ice shell (thin black line). The radiogenic heat production is shown as the thin dashed line and the power required to drive a core dynamo (Eq. (4)) is indicated with a dotted line. In each panel, the gray shaded region indicates the period of Laplace-like resonance passage.

orbital period of Ganymede is ~7 days, thus minimal tidal dissipation occurs. Increasing the magnitude of tidal dissipation in the silicates therefore requires significantly lower silicate effective viscosities. For a typical convective scaling, the heat flux goes as $F_{\text{conv}} \propto 1/\eta_e^{1/3}$. However, for a Maxwell rheology the tidal dissipation goes as $F_{\text{tidal}} \propto 1/\eta_e$. Thus any increase in temperature (or decrease in viscosity) increases the tidal dissipation more than it increases the heat flux, providing the potential for thermal runaway to occur. Decreasing the viscosity does not, however, insure a thermal runaway. Runaway can only occur if the magnitude of the tidal dissipation becomes large enough (relative to radiogenic heating) to dominate the silicate energy balance.

Several factors can contribute to decreasing the effective silicate viscosity. The grain size of the silicates is poorly constrained, with plausible values ranging from 100 μm to 10 cm (Karato, 1984). The choice of grain size can potentially have a profound effect on the model results. Not only do changes in the grain size affect the calculated viscosity (Eq. (15)), but they can also change the dominant rheological flow mechanism: diffusion creep dominates if grains are small, dislocation creep dominates if grains are large. Such a change fundamentally alters the rate at which silicate cooling occurs. Additionally, we have already seen that the composition of Ganymede's mantle strongly affects its thermal history. Olivine is the primary constituent of Earth's mantle and its rheology has been widely studied. It is therefore a reasonable choice for modeling the rheology of Ganymede's mantle. Furthermore, Ganymede's high degree of differentiation (Anderson et al., 1996) is consistent with a dehydrated silicate composition (Kuskov and Kronrod, 2001; Sohl et al., 2002) suggesting dry rheologies are likely. Despite this, the uncertainty in the composition and rheology of Ganymede's silicates warrants an evaluation of whether use of an alternate rheology can increase tidal dissipation.

We performed a suite of simulations that varied the silicate grain size for both dry and wet olivine rheologies. These simulations use a core sulfur mass fraction of 10%. For the dry rheology, decreasing the grain size from 1 mm to 100 μm permits diffusion creep to dominate the flow, decreasing the effective viscosity and causing more rapid cooling to occur. The resulting thermal history is similar to that for a wet olivine rheology with a 1 mm grain size (Fig. 3). For grain sizes larger than or equal to 1 mm dislocation creep dominates the flow and silicate temperatures do not differ noticeably from the simulation described in Section 3.2 (Fig. 5). For a wet rheology, dislocation creep dominates at grain sizes of 1 mm or greater and results in a thermal history essential identical to that shown in Fig. 3. Diffusion creep dominates at grain sizes of 100 μm, and results in even more rapid cooling of the silicate layer. However, while grain size and rheology affect the thermal history of the satellite, no combination of parameters permitted significantly increased tidal dissipation or triggered a thermal runaway in the silicate mantle. The thermal histories are therefore essentially identical to those described in Figs. 2 and 3. Interestingly, if the effective silicate viscosity is arbitrarily decreased by an order of magnitude below that of wet olivine, thermal runaway *can* occur. In this case, core cooling is buffered until resonance passage ends at which point rapid core cooling consistent with magnetic field generation occurs. The above results indicate, however, that variations in grain size cannot accommodate such a large decrease in viscosity. Our basic conclusion, that tidal dissipation in Ganymede's silicate mantle does not enable magnetic field generation, is therefore robust to variations in grain size and assumed rheology.

3.2.2. Variations in Q_J

The tidal dissipation factor of Jupiter (Q_J) is a poorly constrained quantity. The current semi-major axis of Io places a lower bound of 4×10^4 on its time-averaged value (Goldreich and Soter, 1966; Yoder and Peale, 1981); however, theoretical mechanisms for achieving the low values necessary for tidal evolution (10^5 or 10^6) allow Q_J to periodically drop to lower values (10^3 or 10^4) for short spans of time (Ioannou and Lindzen, 1993; Stevenson, 1983). We must therefore consider the degree to which

Author's personal copy

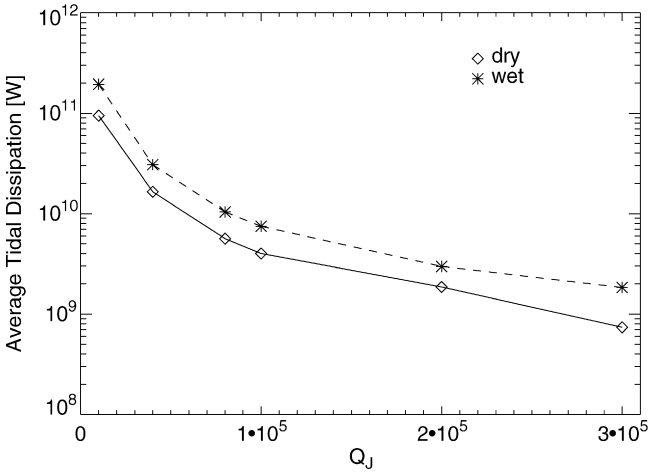

Fig. 6. Average tidal dissipation in the silicate mantle during resonance passage as a function of the tidal dissipation factor of Jupiter for a dry (diamonds) and wet (asterisks) rheology. The silicate grain size is 1 mm.

the above results depend on Q_J. We performed a series of simulations identical to the ones above but with lower values of Q_J. While using low values of Q_J that are constant over the history of the Solar System is physically unrealistic, here we seek only to test the sensitivity of our model results to its assumed value.

Decreasing Q_J produces greater tidal dissipation within Ganymede's silicate layer (Fig. 6). For $Q_J = 10^4$ the average tidal dissipation during resonance passage is 9.5×10^{10} W in the case of a dry rheology and 1.9×10^{11} W in the case of a wet rheology. The decrease in the magnitude of the average tidal dissipation with increasing Q_J varies roughly as $1/Q_J$ as expected from analytical models (Ojakangas and Stevenson, 1986). Despite the relatively high values of tidal dissipation that can occur at low Q_J, tidal dissipation remains insufficient to produce a thermal runaway in the silicate mantle. Thus, the conclusion that resonance passage has not contributed to the production of the current-day magnetic field (Section 3.2) is independent of the assumed value of Q_J. These results are again independent of the assumptions of grain size and composition of the silicates as described above (Section 3.2.1). For completeness we note that variations in Q_J do strongly affect the thermal history of the ice shell. We discuss these effects in a companion paper (Bland et al., submitted for publication).

3.2.3. The influence of the ice shell

The structure of Ganymede's ice shell can strongly influence the magnitude of tidal dissipation in Ganymede's silicates and thus might play an essential role in driving Ganymede's magnetic field. Showman and Malhotra (1997) showed that, for a given Q_J the magnitude of the tidal dissipation saturates at a maximum value if $Q_3/Q_J \lesssim 10^{-3}$. Thus, as long as Q_3/Q_J remains small the total power dissipated is independent of Q_3 (see their Fig. 7). However, the partitioning of tidal energy between the satellite's ice shell and silicate mantle depends on each layer's physical parameters. Thus, if the ice is dissipative (i.e. it has a low viscosity) the majority of the tidal dissipation will occur in the ice. In contrast, if the ice is not dissipative (i.e. it has a high viscosity) the eccentricity is large and more tidal dissipation occurs in the silicate mantle. Here we address the question of whether the physical conditions of Ganymede's ice shell (i.e. grain size and total volume) might allow greater tidal dissipation to occur in Ganymede's silicates.

Fig. 7A shows the total tidal dissipation during resonance passage ($\dot{E}_{\rm sil} + \dot{E}_I$) as a function of the grain size of the ice shell. In these simulations $Q_J = 10^5$. Here, grain size acts as a proxy for Q_3, where large grain sizes correspond to high Q_3 and small grain sizes to low Q_3. Also shown is Ganymede's average eccentricity (e_3) as a function of ice grain size. For small grain sizes (low Q_3), the magnitude of the tidal dissipation remains constant, consistent with Showman and Malhotra (1997). However, as the ice grain size increases and the ice becomes less dissipative the total tidal dissipation within the satellite decreases and Ganymede's maximum eccentricity increases, consistent with previous couple orbital-thermal evolution models (e.g. Ojakangas and Stevenson, 1986). Thus, in these simulations, tidal dissipation is not entirely independent of Q_3.

Despite this limitation, Fig. 7B illustrates that both the absolute magnitude of the power dissipated in the silicates, and the magnitude relative to the total power dissipated in the satellite, increases as a function of ice grain size. In these simulations, only the ice grain size has been changed; the silicate grain size was held constant at 1 mm. At small ice grain sizes where ice is strongly dissipative, very little dissipation occurs in the silicate layer relative to the ice layer. However, as the ice grain size increases and the ice becomes less dissipative relatively more dissipation occurs in the silicates until, at very large grain sizes, essentially all of the tidal dissipation occurs in the silicates. Thus, in spite of the order of magnitude decrease in the total tidal dissipation, an order of magnitude more tidal dissipation occurs in the silicate layer when the ice has a large grain size (100 mm) than when the ice layer has a moderate grain size (1 mm, the nominal case).

The grain size of the ice is not the only parameter that affects the magnitude of tidal dissipation in the silicates. Extensive melting of the ice shell can allow significantly more dissipation to occur in the silicate mantle. Fig. 7C illustrates this effect. The larger the ocean, the less the ice available in which tidal dissipation can occur. When nearly all the ice has melted the majority of the tidal dissipation *must* occur in the silicate mantle. We note that a cold, non-dissipative, ocean-free ice shell would allow even greater dissipation in the silicates (Tobie et al., 2005); however, such a cold ice layer cannot be maintained over a warm silicate mantle. We again emphasize that these results are valid only if the average value of Q_3 remains small relative to Q_J.

Clearly, the ideal ice-shell structure for increasing tidal dissipation in the silicates requires an expansive ocean and a large grain size in the residual ice. To investigate whether the tidal dissipation produced in such a scenario can trigger a thermal runaway in the silicates we simulated Ganymede's thermal history with a 10 cm ice grain size, an ocean adiabat that increases rapidly with depth, and a low Q_J of 4×10^4. The steep ocean adiabat and the low Q_J value permit complete melting of Ganymede's high pressure ice. Both dry and wet silicate rheologies were investigated. During resonance passage the magnitude of tidal dissipation in the silicates reached values as high as 3×10^{11} W (dry rheology) and 7×10^{11} W (wet rheology), but such dissipation again remained incapable of causing a thermal runaway. Thus, even the most favorable ice shell conditions cannot force enough tidal dissipation to occur in the silicates to allow a thermal runaway that can prevent the core from cooling during resonance passage.

3.2.4. Partial melt

The temperature of Ganymede's silicate mantle shown in Figs. 2–5 are in excess of the solidus temperature of olivine at the pressures typical of Ganymede's silicate layer (~1650 K; Takahashi, 1990; Breuer and Spohn, 2006). We therefore expect partial melting to occur. Partial melting has two primary effects. First, melting of the rocky material absorbs latent heat from the system, buffering temperature increases in a manner analogous to ocean formation in the ice shell (Fig. 5A). Second, the presence of even a few percent partial melt can have a profound effect on the rheology, decreasing the effective viscosity by an order of magnitude or more (Kohlstedt and Zimmerman, 1996; Jin et al., 1994). Because the rate of tidal dissipation is strongly de-

Author's personal copy

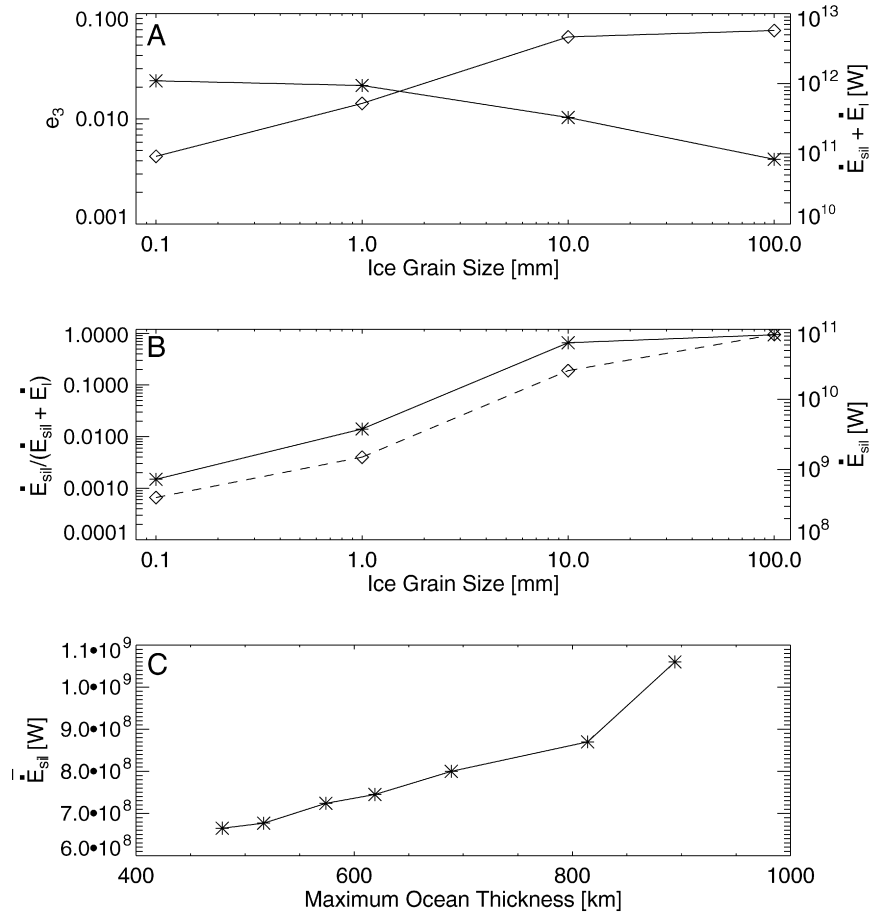

Fig. 7. (A) The average eccentricity of Ganymede (e_3) during resonance passage (diamonds) and the average total tidal dissipation in the satellite ($\dot{E}_{sil} + \dot{E}_I$ in W) during resonance passage (asterisks) as a function of ice grain size. Large ice grain sizes increase Q_3, decreasing the total tidal dissipation and increasing the satellite's eccentricity. (B) The magnitude of the tidal dissipation in the silicates ($\dot{E}_{sil}$, solid line) and the magnitude relative to the tidal dissipation in the whole satellite ($\dot{E}_{sil} + \dot{E}_I$, dashed line) as a function of ice grain size. Despite the decrease in total tidal dissipation within the satellite (see A), the magnitude of tidal dissipation in the silicates increases as the ice becomes less dissipative. (C) Average tidal dissipation ($\bar{\dot{E}}_{sil}$ in W) in the silicates during the period of resonance passage as a function of maximum ocean thickness. For an ocean thickness of ~900 km complete melting of the high pressure ice occurs. The ocean thickness was varied by modifying the thermal adiabat assumed for Ganymede's ocean. The ice grain size was 1 mm in each simulation.

pendent on the viscosity of the material, the decrease in silicate viscosity associated with partial melting may allow increased dissipation in the silicates. If the magnitude of the dissipation is large enough, mantle temperatures may be maintained at the melting temperature throughout resonance passage. Rapid silicate and core cooling would then follow resonance escape.

To evaluate whether the inclusion of partial melt helps enable magnetic field generation we performed a suite of simulations that account for the effect of latent heating on the thermal balance of the silicates. In these simulations, if temperatures exceed 1652 K (the solidus temperature at a pressure of 2 GPa) we modify the thermal balance (Eq. (6)) to include the latent heat of melting as follows

$$\frac{4}{3}\pi\left(R_{sil}^3 - R_c^3\right)\rho_{sil}H + 4\pi R_c^2 F_c + \dot{E}_{sil} = 4\pi R_{sil}^2 F_{sil} + \left[M_{melt}\frac{df}{dT}L_{sil} + \frac{4}{3}\pi\left(R_{sil}^3 - R_c^3\right)\rho_{sil}c_{p,sil}\right]\frac{dT_{sil}}{dt}, \quad (25)$$

where M_{melt} is the mass of the melt region, df/dT is the increase in melt fraction per Kelvin, and L_{sil} is the latent heat of olivine. The mass of the melt region, M_{melt}, is determined by equating the olivine solidus curve ($T_{sol} = 1409. + 134.2P - 6.581P^2 + 0.1054P^3$, where P is the pressure in GPa; Takahashi, 1990; Breuer and Spohn, 2006) to a mantle adiabat of the form $dT/dP = (\alpha_{sil}T)/(\rho_{sil}c_{p,sil})$ and solving for the depth at which the curves intersect, assuming hydrostatic equilibrium. The resulting melt region volume is then converted to a mass assuming a constant density mantle. The change in melt fraction with temperature, df/dT, is determined from the olivine solidus and liquidus curves assuming a simple linear relationship between melt fraction and temperature (Jaques and Green, 1980). In addition, we reduce the silicate viscosity calculated from Eq. (15) by a factor of 10 if partial melt is present.

Once the melt fraction exceeds 3% (the maximum amount of melt permissible before melt separation occurs; McKenzie and Bickle, 1988), we assume that melt is extracted from the mantle and erupted at the base of the ice shell. We make the simplifying assumption at this point that the energy balance of the silicates is not dominated by changes in temperature (which is now held fixed) but by the production and removal of melt. In addition, the eruption of melt at the base of the ice shell alters the energy balance of the ice layer. A more complex thermal balance, such as that suggested by Moore (2001), is beyond the immediate scope of this feasibility study.

Fig. 8 shows the temperature of the silicate mantle and metallic core, and the core cooling rate as a function of time for a simulation that includes partial melting. The simulation utilizes a wet silicate rheology with a grain size of 1 mm. Additionally, we use a low, constant Q_J of 4×10^4 to test the maximum plausible rate

Author's personal copy

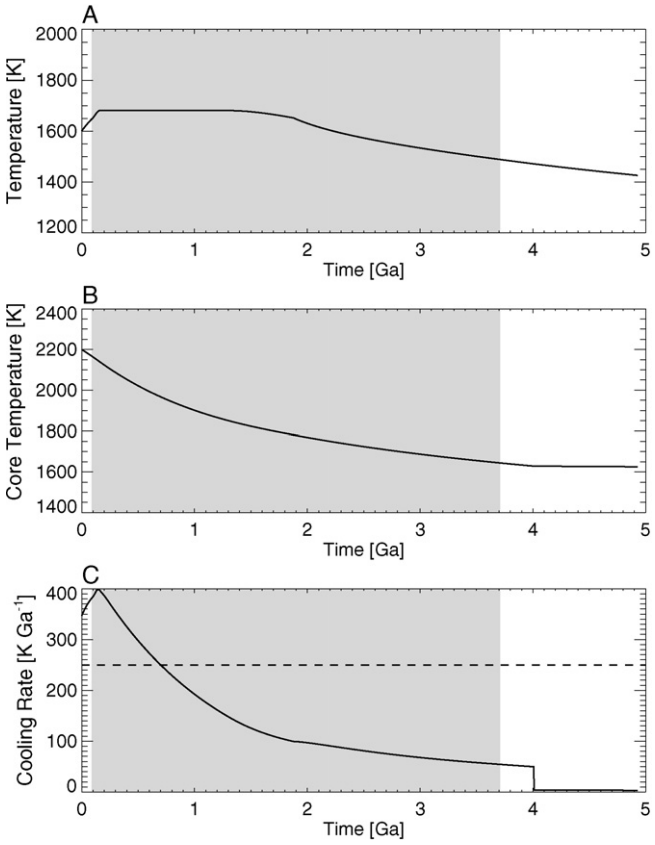

Fig. 8. Temperatures in Ganymede's silicate mantle (A) and core (B), and the core cooling rate (C) as a function of time for a simulation that includes partial melting in the silicate mantle. The simulation utilizes a wet rheology with a grain size of 1 mm. Initial silicate and core temperatures were 1600 K and 2200 K, respectively. $Q_J = 4 \times 10^4$ for the entire simulation. The shaded region indicates the period of Laplace-like resonance passage.

of tidal dissipation. We initialize the simulation with low silicate temperatures (1600 K) to avoid *a priori* assumptions regarding initial quantities of partial melt. Silicate temperatures initially rise rapidly due to radiogenic heating until reaching a temperature of 1652 K, at which point partial melting slows the increase in silicate temperatures. The melt fraction quickly reaches 3% and the silicate temperatures saturate, with melt production and removal dominating the thermal balance. After 1.4 Ga the melt fraction falls below 3% and the silicate mantle begins to cool. However, this cooling is still reduced by the latent heat of freezing of the silicate melt. The buffering of the silicate cooling briefly keeps silicate temperatures above the values expected if they were in quasiequilibrium with radiogenic heating. Thus, once all the melt has solidified, the silicates cool rapidly to come back into quasiequilibrium with radiogenic heat. During this brief cooling period silicate cooling rates can reach values as high as 200 $\mathrm{K\,Ga^{-1}}$. This rapid cooling occurs *in spite* of the satellite being in the Laplace-like resonance. Thus, tidal heating again is unable to prevent core cooling.

The insufficient buffering of core cooling is further illustrated in Figs. 8B and 8C. The core cooling rate is initially quite high and core temperatures drop rapidly. This is due to the large difference between the initial core and mantle temperatures. After 0.7 Ga the core cooling rate drops below the requirement for thermal convection and never again attains such large values. At 4.1 Ga inner core growth begins and the core cooling rate approaches zero. Magnetic field production by chemical convection is possible during this period, but is subject to the same constraints described in Section 3.1. Fig. 8 clearly illustrates that, like the simulations described above, resonance passage is unable to modify the thermal history of the metallic core or silicate mantle when partial melt is included.

3.3. The timing of core formation

All of the simulations described above assume that Ganymede differentiated early and that its silicate mantle and metallic core are initially hot. However, several authors have shown that metallic core formation in a large icy satellite can take an additional 1 to 2 Ga after initial differentiation of ice and rock (Grasset et al., 2000; Schubert et al., 2004). The simulations described above can therefore be considered an end member scenario in which complete differentiation occurs rapidly. In light of the stringent compositional requirements on chemical convection and the failure of tidal dissipation to delay or prolong thermal convection in the metallic core, late core formation may provide a mechanism by which magnetic field production is delayed until the present day. If the core is young, it may still be cooling rapidly enough for thermal convection to drive a magnetic dynamo.

As a preliminary test of the feasibility of dynamo generation by a young core we performed a series of simulations in which the radiogenic heating was initialized as if 1 or 2 Ga of decay had already occurred, mimicking late core formation. For simplicity these simulations did not include the partial melting described in Section 3.2.4. As with the resonance passage models, these simulations failed to produce cooling rates consistent with a present day thermally generated dynamo. Our simplified modeling therefore suggests that late core formation cannot explain the existence of Ganymede's magnetic field. However, we have neglected the process of core formation itself which may substantially modify the thermal and physical conditions of both the metallic core and silicate mantle. If, for example, core formation produced a metallic core significantly hotter than the mantle above (cf. Solomatov and Ke, 2007), sustained thermal convection and dynamo action may occur easily. Thus, detailed modeling of metallic core formation is required to fully assess the potential for magnetic field production in a late-formed core. Late core formation therefore remains a potential mechanism for enabling present day dynamo action.

4. Conclusions

We have shown that production of Ganymede's magnetic field by secular cooling and chemical convection requires that a very specific set of conditions be met: the mass fraction of sulfur in the core must be low (or alternatively very high), the core must have formed hot, and the silicate mantle must be able to cool rapidly (i.e. it must have a viscosity consistent with wet olivine). If any of these criterion are not met magnetic field production fails. These results contrast with previous workers who find that compositional convection can drive a core dynamo under a broad range of conditions (Hauck et al., 2006).

Because of the stringent conditions required for operation of a chemically driven dynamo, we investigated whether a period of tidal dissipation in Ganymede's past might enable production of the current magnetic field under a broader range of conditions. We have shown here, however, that passage through a Laplace-like resonance is insufficient to cause substantial tidal dissipation within Ganymede's silicate mantle. The cooling history of Ganymede's core is therefore unaffected by the satellite's orbital history and the presence of Ganymede's magnetic field cannot be attributed to resonance passage as suggested by previous authors (Stevenson, 1996; Showman et al., 1997). Modifying the rheology and grain size of the silicates, decreasing the value of Q_J, varying the structure of the ice shell, and allowing for partial melting all modify the thermal history of the satellite. However, no simulations were found

Author's personal copy

that broaden the conditions under which magnetic field generation is predicted. The simulations described above examine passage through the Laplace-like resonance that most strongly pumps Ganymede's eccentricity ($\omega_1/\omega_2 = 2$); thus, other orbital histories that pass through weaker Laplace-like resonances ($\omega_1/\omega_2 = 3/2$ or $1/2$) are also unlikely to enable Ganymede's magnetic field.

Considering the difficulty of explaining Ganymede's magnetic field, is there another alternative? One possibility is that Ganymede differentiated late in its history. The discovery that Callisto may be only partially differentiated (Anderson et al., 1997) has lead to the development of satellite formation models that allow for slow, cool satellite accretion that avoids early differentiation (e.g. Canup and Ward, 2002). While these models explain Callisto's partially differentiated state, they may also require that Ganymede formed partially differentiated [though see Mosqueira and Estrada (2003), who simultaneously form an undifferentiated Callisto in the gas-poor region of Jupiter's extended subnebula, but rapidly form a differentiated Ganymede in the optically thick region of the disk]. If the slow, cool, accretion scenario of Canup and Ward (2002) is assumed, then Ganymede's current highly condensed state suggests that differentiation may have occurred later, perhaps during passage through one or more of the Laplace-like resonances described above. In such a scenario Ganymede's metallic core may have formed late in its history, and might therefore still be cooling convectively. The thermal modeling described above suggests that such thermal convection is only possible if the core formed hot relative to the silicates above it, and even then convection will only occur within the first 1 Ga of core formation. Such late core formation is marginally consistent with age of Ganymede's grooved terrain (thought to be 1 to 2 Ga; Zahnle et al., 2003), which may have formed during the same differentiation event. Late core formation may therefore provide an alternative mechanism for production of Ganymede's magnetic field.

Acknowledgments

This work was supported by NASA Headquarters under the NASA Earth and Space Science Fellowship Program—Grant #NNX07AV22H and NASA PG&G Grant #NNX07AR27G. The authors thank Renu Malhotra for use of the orbital dynamics code. Hauke Hussmann and an anonymous reviewer provided thoughtful reviews that strengthened the manuscript.

References

Anderson, J.D., Lau, E.L., Sjogren, W.L., Schubert, G., Moore, W.B., 1996. Gravitational constraints on the internal structure of Ganymede. Nature 384, 541–543.

Anderson, J.D., Lau, E.L., Sjogren, W.L., Schubert, G., Moore, W.B., 1997. Gravitational evidence for an undifferentiated Callisto. Nature 387, 264–266.

Boehler, R., 1996. Fe–FeS eutectic temperatures to 620 kbar. Phys. Earth Planet. Int. 96, 181–186.

Braginsky, S.I., 1963. Structure of the F-layer and reasons for convection in Earth's core. Dokl. Akad. Nauk SSSR 149, 8–10.

Breuer, D., Spohn, T., 2006. Viscosity of the martian mantle and its initial temperature: Constraints from crust formation history and the evolution of the magnetic field. Planet. Space Sci. 54, 153–169.

Buffett, B.A., 2002. Estimates of heat flow in the deep mantle based on the power requirements for the geodynamo. Geophys. Res. Lett. 29, 7.

Buffett, B.A., Huppert, H.E., Lister, J.R., Woods, A.W., 1996. On the thermal evolution of the Earth's core. J. Geophys. Res. 101, 7989–8006.

Canup, R.M., Ward, W.R., 2002. Formation of the Galilean satellites: Conditions of accretion. Astron. J. 124, 3404–3423.

Christensen, U.R., Aubert, J., 2006. Scaling properties of convection-driven dynamos in rotating spherical shells and application to planetary magnetic fields. Geophys. J. Int. 166, 97–114.

Crary, F.J., Bagenal, F., 1998. Remanant ferromagnetism and the interior structure of Ganymede. J. Geophys. Res. 103, 25757–25773.

Fei, Y., Bertka, C.M., Finger, L.W., 1997. High-pressure iron-sulfur compound, Fe_3S_2, and melting relations in the Fe–FeS system. Science 275, 1621–1623.

Fischer, H.J., Spohn, T., 1990. Thermal-orbital histories of viscoelastic models of Io (JI). Icarus 83, 39–65.

Freeman, J., 2006. Non-Newtonian stagnant lid convection and the thermal evolution of Ganymede and Callisto. Planet. Space Sci. 54, 2–14.

Goldreich, P., Soter, S., 1966. Q in the Solar System. Icarus 5, 375–389.

Goldsby, D.L., Kohlstedt, D.L., 2001. Superplastic deformation of ice: Experimental observations. J. Geophys. Res. 106, 11017–11030.

Grasset, O., Sotin, C., Deschamps, F., 2000. On the internal structure and dynamics of Titan. Planet. Space Sci. 48, 617–636.

Greenberg, R., 1987. Galilean satellites: Evolutionary paths in deep resonance. Icarus 70, 334–347.

Gubbins, D., 1977. Energetics of the Earth's core. J. Geophys. 43, 453–464.

Gubbins, D., Alfè, D., Masters, G., Price, G.D., Gillan, M., 2004. Gross thermodynamics of two-component core convection. Geophys. J. Int. 157, 1407–1414.

Gurnett, D.A., Kurth, W.S., Roux, A., Bolton, S.J., Kennel, C.F., 1996. Evidence for a magnetosphere at Ganymede from plasma wave observations by the Galileo spacecraft. Nature 384, 535–537.

Hauck, S.A., Aurnou, J.M., Dombard, A.J., 2006. Sulfur's impact on core evolution and magnetic field generation on Ganymede. J. Geophys. Res. 111, doi:10.1029/2005JE002557. E09008.

Hersant, F., Gautier, D., Lunine, J.I., 2004. Enrichment in volatiles in the giant planets of the Solar System. Planet. Space Sci. 52, 623–641.

Hussman, H., Spohn, T., 2004. Thermal-orbital evolution of Io and Europa. Icarus 171, 391–410.

Ioannou, P.j., Lindzen, R.S., 1993. Gravitational tides in the outer planets. II. Interior calculations and estimation of the tidal dissipation factor. Astrophys. J. 406, 266–278.

Jaques, A.L., Green, D.H., 1980. Anhydrous melting of peridotite at 0–15 Kb pressure and the genesis of tholeiitic basalt. Contrib. Mineral. Petrol. 73, 287–310.

Jin, Z., Green, H.W., Zhou, Y., 1994. Melt topology in partially molten mantle peridotite during ductile deformation. Nature 372, 164–167.

Karato, S., 1984. Grain-size distribution and rheology of the upper mantle. Tectonophysics 104, 155–176.

Karato, S., Wu, P., 1993. Rheology of the upper mantle. Science 260, 771–778.

Khurana, K.K., Kivelson, M.G., Stevenson, D.J., Schubert, G., Russell, C.T., Walker, R.J., Polanskey, C., 1998. Induced magnetic fields as evidence for subsurface oceans in Europa and Callisto. Nature 395, 777–780.

Kirk, R.L., Stevenson, D.J., 1987. Thermal evolution of a differentiated Ganymede and implications for surface features. Icarus 69, 91–134.

Kivelson, M.G., Khurana, K.K., Russell, C.T., Walker, R.J., Warnecke, J., Coroniti, F.V., Polanskey, C., Southwood, D.J., Schubert, G., 1996. Discovery of Ganymede's magnetic field by the Galileo spacecraft. Nature 384, 537–541.

Kivelson, M.G., Khurana, K.K., Coroniti, F.V., Joy, S., Russell, C.T., Walker, R.J., Warnecke, J., Bennett, L., Polanskey, C., 1997. The magnetic field and magnetosphere of Ganymede. Geophys. Res. Lett. 24, 2155–2158.

Kivelson, M.G., Warnecke, J., Bennett, L., Joy, S., Khurana, K.K., Linker, J.A., Russell, C.T., Walker, R.J., Polanskey, C., 1998. Ganymede's magnetosphere: Magnetometer overview. J. Geophys. Res. 103, 19963–19972.

Kivelson, M.G., Khurana, K.K., Stevenson, D.J., Bennett, L., Joy, S., Russell, C.T., Walker, R.J., Zimmer, C., Polanskey, C., 1999. Europa and Callisto: Induced or intrinsic fields in a periodically varying plasma environment. J. Geophys. Res. 104, 4609–4626.

Kivelson, M.G., Khurana, K.K., Russell, C.T., Volwerk, M., Walker, R.J., Zimmer, C., 2000. Galileo magnetometer measurements: A stronger case for a subsurface ocean at Europa. Science 289, 1340–1343.

Kivelson, M.G., Khurana, K.K., Russell, C.T., Joy, S.P., Volwerk, M., Walker, R.J., Zimmer, C., Linker, J.A., 2001. Magnetized or unmagnetized: Ambiguity persists following Galileo's encounters with Io in 1999 and 2000. J. Geophys. Res. 106, 26121–26136.

Kivelson, M.G., Khurana, K.K., Volwerk, M., 2002. The permanent and inductive magnetic moments of Ganymede. Icarus 157, 507–522.

Kohlstedt, D.L., Zimmerman, M.E., 1996. Rheology of partially molten mantle rocks. Annu. Rev. Earth Planet. Sci. 24, 41–62.

Kuang, Z., Stevenson, D.J., 1996. Magnetic field generation in the Galilean satellites. Eos (Fall Suppl.) 77 (46), F437.

Kuskov, O.L., Kronrod, V.A., 2001. Core sizes and internal structure of Earth's and Jupiter's satellites. Icarus 151, 204–227.

Lewis, J.S., 1982. Io: Geochemistry of sulfur. Icarus 50, 103–114.

Lister, J.R., Buffett, B.A., 1995. The strength and efficiency of thermal and compositional convection in the geodynamo. Phys. Earth Planet. Int. 91, 17–30.

Loper, D.E., 1975. Torque balance for precessionally driven dynamos. Phys. Earth Planet. Int. 11, 43–60.

Loper, D.E., 1978a. Some thermal consequences of a gravitationally powered dynamo. J. Geophys. Res. 83, 5961–5970.

Loper, D.E., 1978b. The gravitationally powered dynamo. Geophys. J. R. Astron. Soc. 54, 389–404.

Malhotra, R., 1991. Tidal origin of the Laplace resonance and the resurfacing of Ganymede. Icarus 94, 399–412.

Malkus, W.V.R., 1963. Precessional torques as the cause of geomagnetism. J. Geophys. Res. 68, 2871–2886.

McKenzie, D., Bickle, M.J., 1988. The volume and composition of melt generated by extension of the lithosphere. J. Petrol. 29, 625–679.

Author's personal copy

McKinnon, W.B., 1996. Core evolution in the icy satellites, and the prospects for dynamo-generated magnetic fields. Bull. Am. Astron. Soc. 28, 1076.
McKinnon, W.B., 2006. Differentiation of the Galilean satellites: It's Different out there. In: Workshop on Early Planetary Differentiation, LPI Contributions 1335, pp. 66–67.
McKinnon, W.B., Desai, S., 2003. Internal Structures of the Galilean satellites: What can we really tell? Lunar Planet. Sci. 34. Abstract #2104.
Moore, W.B., 2001. The thermal state of Io. Icarus 154, 548–550.
Mosqueira, I., Estrada, P.R., 2003. Formation of the regular satellites of giant planets in an extended gaseous nebula. I. Subnebula model and accretion of satellites. Icarus 163, 198–231.
Mousis, O., Alibert, Y., 2006. Modeling the jovian subnebula. II. Composition of regular satellite ices. Astron. Astrophys. 448, 771–778.
Ojakangas, G.W., Stevenson, D.J., 1986. Episodic volcanism of tidally heated satellites with application to Io. Icarus 66, 341–358.
Olson, P., Christensen, U.R., 2006. Dipole moment scaling for convection-driven planetary dynamos. Earth Planet. Sci. Lett. 250, 561–571.
Pasek, M.A., Milsom, J.A., Ciesla, F.J., Lauretta, D.S., Sharp, C.M., Lunine, J.I., 2005. Sulfur chemistry with time-varying oxygen abundance during Solar System formation. Icarus 175, 1–14.
Peale, S.J., 1999. Origin and evolution of the natural satellites. Annu. Rev. Astron. Astrophys. 37, 533–602.
Peale, S.J., Lee, M.H., 2002. A primordial origin of the Laplace relation among the Galilean satellites. Science 298, 593–597.
Petrenko, V.F., Whitworth, R.W., 1999. Physics of Ice. Oxford University Press, Oxford.
Ranalli, G., 1995. Rheology of the Earth. Chapman & Hall, London.
Reese, C.C., Solomatov, V.S., Baumgardner, J.R., 2005. Scaling laws for time-dependent stagnant lid convection in a spherical shell. Phys. Earth Planet. Int. 149, 361–370.
Rochester, M.G., Jacobs, J.A., Smylie, D.E., Chong, K.R., 1975. Can precession power the geodynamo? Geophys. J. R. Astron. Soc. 43, 661–678.
Sarson, G.R., Jones, C.A., Zhang, K., Schubert, G., 1997. Magnetoconvection dynamos and the magnetic fields of Io and Ganymede. Science 276, 1106–1108.
Schubert, G., Ross, M.N., Stevenson, D.J., Spohn, T., 1988. Mercury's thermal history and the generation of its magnetic field. In: Vilas, F., Chapman, C.R., Matthews, M.S. (Eds.), Mercury. University of Arizona Press, Tucson, pp. 429–460.
Schubert, G., Zhang, K., Kivelson, M.G., Anderson, J.D., 1996. The magnetic field and internal structure of Ganymede. Nature 384, 544–545.
Schubert, G., Anderson, J.D., Spohn, T., McKinnon, W.B., 2004. Interior composition, structure and dynamics of the Galilean satellites. In: Bagnell, F., Dowling, T., McKinnon, W.B. (Eds.), Jupiter. The Planet, Satellites and Magnetosphere. Cambridge University Press, pp. 281–306.
Scott, H.P., Williams, Q., Ryerson, F.J., 2002. Experimental constraints on the chemical evolution of large icy satellites. Earth Planet. Sci. Lett. 203, 399–412.
Showman, A.P., Malhotra, R., 1997. Tidal evolution into the Laplace resonance and the resurfacing of Ganymede. Icarus 127, 93–111.
Showman, A.P., Stevenson, D.J., Malhotra, R., 1997. Coupled orbital and thermal evolution of Ganymede. Icarus 129, 367–383.
Sohl, F., Spohn, T., Breuer, D., Nagel, K., 2002. Implications from Galileo observations on the interior structure and chemistry of the Galilean satellites. Icarus 157, 104–119.
Solomatov, V.S., 1995. Scaling of temperature- and stress-dependent viscosity convection. Phys. Fluids 7, 266–274.
Solomatov, V.S., Barr, A.C., 2006. Onset of convection in fluids with strongly temperature-dependent, power-law viscosity. Phys. Earth Planet. Int. 155, 140–145.
Solomatov, V.S., Barr, A.C., 2007. Onset of convection in fluids with strongly temperature-dependent, power-law viscosity. 2. Dependence on the initial perturbation. Phys. Earth Planet. Int. 165, 1–13.
Solomatov, V.S., Ke, Y., 2007. Coupled core–mantle thermal convection after a giant impact. Eos (Fall Suppl.) 88 (52). Abstract U21D-01.
Solomatov, V.S., Moresi, L.N., 2000. Scaling of time-dependent stagnant lid convection: Application to small-scale convection on Earth and other terrestrial planets. J. Geophys. Res. 105, 21795–21817.
Stevenson, D.J., 1983. Anomalous bulk viscosity of two-phase fluids and implications for planetary interiors. J. Geophys. Res. 88, 2456–2474.
Stevenson, D.J., 1996. When Galileo met Ganymede. Nature 384, 511–512.
Stevenson, D.J., 2003. Planetary magnetic fields. Earth Planet. Sci. Lett. 208, 1–11.
Stevenson, D.J., Spohn, T., Schubert, G., 1983. Magnetism and thermal evolution of the terrestrial planets. Icarus 54, 466–489.
Takahashi, E., 1990. Speculations on the Archean mantle: Missing link between komatiite and depleted garnet peridotite. J. Geophys. Res. 95, 15941–15954.
Tittemore, W.C., 1990. Chaotic motion of Europa and Ganymede and the Ganymede–Callisto dichotomy. Science 250, 263–267.
Tobie, G., Mocquet, A., Sotin, C., 2005. Tidal dissipation within large icy satellites: Applications to Europa and Titan. Icarus 177, 534–549.
Usselman, T.M., 1975. Experimental approach to the state of the core. Part I. The liquidus relations of the Fe-rich portion of the Fe–Ni–S system. Am. J. Sci. 275, 278–290.
Vanyo, J., Wilde, P., Cardin, P., Olson, P., 1995. Experiments on precessing flows in the Earth's liquid core. Geophys. J. Int. 121, 136–142.
Veeder, G.J., Matson, D.L., Johnson, T.V., Blaney, D.L., Goguen, J.D., 1994. Io's heat flow from infrared radiometry: 1983–1993. J. Geophys. Res. 99, 17095–17162.
Verhoogen, J., 1961. Heat balance of the Earth's core. Geophys. J. 4, 276–281.
Wienbruch, U., Spohn, T., 1995. A self sustained magnetic field on Io? Planet. Space Sci. 9, 1045–1057.
Williams, D.J., Mauk, B.H., McEntire, R.W., Roelof, E.C., Armstrong, T.P., Wilken, B., Roederer, J.G., Krimigis, S.M., Fritz, T.A., Lanzerotti, L.J., Murphy, N., 1997. Energetic particle signatures at Ganymede: Implications for Ganymede's magnetic field. Geophys. Res. Lett. 24, 2163–2166.
Yoder, C.F., 1979. How tidal heating in Io drives the Galilean orbital resonance locks. Nature 279, 767–770.
Yoder, C.F., Peale, S.J., 1981. The tides of Io. Icarus 47, 1–35.
Zahnle, K., Schenk, P., Levison, H.F., Dones, L., 2003. Cratering rates in the outer Solar System. Icarus 163, 263–289.
Zimmer, C., Khurana, K.K., Kivelson, M.G., 2000. Subsurface oceans on Europa and Callisto: Constraints from Galileo magnetometer observations. Icarus 147, 329–347.